Combining continuous spatial and temporal scales for SGD investigations using UAV-based thermal infrared measurements

Ulf Mallast[1], Christian Siebert[1]
[1] Helmholtz Centre for Environmental Research -UFZ, T. Lieser Str. 4, Halle 06120, Germany

Correspondence to: Ulf Mallast (ulf.mallast@ufz.de)

Hereafter included are the requested point-by-point response to the reviewers (pgs. 2-12), a list of relevant changes (pg. 13) and the marked-up manuscript version (pgs. 14-48).

Ulf Mallast

Halle, 04.12.2018

Reply to Reviewer 1:

Your evaluation was of particular and valuable importance to improve our manuscript. It is great to have reviewers like you, who spent a lot of time to carefully read through manuscripts and really help to put it onto the next level. Thank you. In the following we would like to comment on a point-to-point basis on the given reviewer comments (reviewer comments are given in bold, answers in given in italic).

Does the paper present novel concepts, ideas, tools, or data?

Yes. This manuscript addresses an important gap in the scientific publication record on Submarine Groundwater Discharge (SGD). Specifically, while SGD has been widely studied over the last decade, almost all studies lack data that can define temporal and spatial scales of SGD precisely. The reviewed presented manuscript successfully aims at accomplishing this. The remote sensing data collected for this study is novel in is presentation and processing.

Thank you for your evaluation. We too think that there is a gap of a combined analysis of temporal and spatial scales of SGD and we hope our study is the onset for further studies that seek to accomplish to bridge that gap similar to what is done in the Near Shore Imaging community.

Are substantial conclusions reached and do the authors give proper credit to related work and clearly indicate their own new/original contribution?

Substantial conclusions are reach in the form of the methodology presented in this manuscript. A processing method is used that can lead to significant help for other studies in identifying SGD hotspots. That said, the authors fail to mention that the presented methodology, while new to thermal image processing, has been used by the Near Shore Imaging community such as the producers of Argus for a while. The authors should not only reference this work (e.g. Holman et al., 2017 and therein https://ieeexplore.ieee.org/document/7809056/) but also change the language of their manuscript to match the existing technical language used in the field.

To be completely honest, up to now, we were not aware of Argus, nor Cosmos, nor any other system, which uses optical camera solutions to monitor beach dynamics, long shore currents or derive near-shore bathymetry. The latter, or more specifically cBathy, by the way, is pretty interesting and could also work with thermal infrared data since wave crests are perfectly visible due to the changed incidence angle and thus the changed emissivity. The suggested work by Holman et al 2017 matches our method and approach in large parts, starting in the idea itself using a fixed camera (whether it is from an UAV platform or from a post), through the creation of a data cube after registering all images (whether it is with fixed GCPs as in the Holman et al. case or with an intensity based image registration system requiring no GCPs at all in the present case), up to the time series analysis of a continuous cross-shore stack of pixels to illustrate a certain geometric variance. Thus, we will certainly cite Holman et al. Concerning the technical language, we will adapt some terms (e.g. time stack, data cube, cross shore scale) mentioned throughout Holman et al. 2017 and earlier Holman publications to match technical language. If reviewer 1 thinks of further terms to be matched, we would be eager to know them and to discuss their integration as well.

Are the scientific methods and assumptions valid and clearly outlined?

The scientific methods are clearly described and valid. They could be better backed up by above mentioned references. A comparison for example between existing Image products in Argus and those presented in this manuscript would be little effort but very effective.

As suggested, we will back up our methods with references from the Near Shore imaging community. In this context, we will discuss Argus product (e.g. Time Series and Trend analysis) and our result/product.

Are the results sufficient to support the interpretations and conclusions?

The results on SGD hotspot identification and current movement are sufficiently supported and deserve publication. That said, I find the conclusion on effects of geology on discharge pulses rather speculative.

Due to missing tomographic investigations of the related geological formation (the dry-fallen lakebed), we have to speculate, that geological effects may force the observed discharge pulses. We propose, due to a randomly developed network of karst structures, discharge effects such as known from pulsating springs/gushers are observed. However, we emphasized in the manuscript that we only propose the maturity of the karst system to be one possible explanation. To be even clearer on that issue we will rework the concluding statement.

There are three potentially minor problems with the conclusion of the manuscript: One: The authors should address the potential problem with utilizing only two reference reflectors (see Fig 1). A plane cannot be established with only two reference points, thereby potentially underestimating the distortion effect a changing plane can have on the recorded pixels. See above mentioned reference. This can easily be incorporated into the manuscript by including a section on "limitations and potential errors", which is already mostly written.

The method we used for co-registration of the slave image onto the master image does not depend on the two reflectors only, but on all rigid land parts (several hundreds of pixels), or more specifically on the similarity of the intensities of both images. Since the rigid land parts are similar in intensity in master and slave images, the rigid land parts will be the only image part taken into account

In a first step, the similarity matrix between the two images is calculated. Incorporating scaling, rotation and translation, in a second step, the slave image is iteratively transformed and each time compared to the master image using the similarity between the master and the transformed slave image. The similarity "goodness" is evaluated each time using a mean square metric (which we chose to be a regular step gradient descent) as accuracy measure. As long as neither the maximum iteration criterion is reached (in our case 1000 iterations), nor the quality criterion (in our case a Maximum Step Length of 1.0e-2) the optimization process is continued until one of the two criteria is reached.

This process is repeated for all slave images. To provide a further independent measure accuracy measure we used the two reflectors. Similar to the automatic approach describe in Holman et al. 2017 to find GPS targets, we defined the search windows in the co-registered images looking for the lowest radiance values (=reflector plates). Since the plates represent an area of several connected pixel we then extracted the mass centre of both plates and compared the coordinates of the mass

centre to the coordinates of the mass centre (reflector plates) of the master image, getting the spatial accuracy among images (Fig. S1), giving us a criterion on how to evaluate spatiotemporal changes in the light of image registration uncertainties. Thus, we are convinced distortion effects due to the image registration process to be minor in the presented case. For reproducing purposes however, as suggested, we will add, a section "Limitations and Potential Errors" picking up possible distortion effect with less land parts, and other possible pitfalls hindering a successful reproduction of the proposed method.

Two: The authors must include a discussion of bathymetry and it's potential effect on the data in a more comprehensive way. Is the substrate flat etc.

We added a more comprehensive discussion concerning the bathymetry in the revised version of the manuscript.

Three: In section 4.3 the authors write "In this context the question arises on the transferability of the presented approach" but they don't give a qualitative answer to this question. A short discussion on how the results may vary in SGD studies that don't have the extreme buoyancy differences should be included.

We agree and will elaborate on transferability, possibly within the newly created section "Limitations and Potential Errors".

Is the description of experiments and calculations sufficiently complete and precise to allow their reproduction by fellow scientists (traceability of results)?

Yes.

Does the title clearly reflect the contents of the paper?

Yes, but it is a bit technical.

If the reviewer doesn't mind, we would keep the title as it is.

Does the abstract provide a concise and complete summary?

Yes.

Is the overall presentation well structured and clear?

The overall structure is clear and follows a clear structure. That said, there is a significant typo in the manuscript. What is labeled as Methods is actually Results.

Thank you and yes we agree, there is a significant typo that is already corrected. After having been pinpointed to this typo we encountered further numbering mistakes in headings (e.g. 4.3 occurs twice) and figures. All of them are already corrected, but will be double-checked again before submitting the revised version.

Is the language fluent and precise?

NO!! There are significant problems with the language. The manuscript is speckled with syntax and grammatical mistakes. While I have the utmost level of sympathy for this issue the authors should utilize the help of a professional editor. There are a number of logical problems in this manuscript that I believe are a result of the significant language problems displayed in this manuscript. Also, there are many subjective or judgmental adjectives in the manuscript (i.e. the use of the word "clear" or "clearly" is used 20 times alone in the manuscript). All of them should be eliminated. All this being said, in light of the very high value of the content of this manuscript I still consider this problem to be minor and easily fixed. I wanted to assist in this task and have attached a PDF where I have marked up some of the most obvious mistakes.

We are infinitely grateful for the very detailed improvements reviewer 1 gave in his/her attachment. This sort of assistance, that most certainly demanded an enormous amount of time, can no one expect and is rarely offered to push the overall value of the submitted manuscript beyond the content-based value. Again, we really appreciate the efforts of reviewer 1, will of course incorporate his/her suggestions, and will also utilize the help of a professional editor.

Are mathematical formulae, symbols, abbreviations, and units correctly defined and used?

For the most part yes. There is an inconsistency in the use of the symbol "~". For example it says on Page 7 Section 2 (which is actually Section 3) "~20 to ~46 pixels (2.6m-6.0). If the pixels is inexact then the measure of meters must be to. The same applies for the rest of the manuscript. Consistency is lacking in the use of abbreviated unites and spelled out unites, i.e. seconds and m.

True, we will rework the consistency aspect.

Should any parts of the paper (text, formulae, figures, tables) be clarified, reduced, combined, or eliminated?

Yes, large sections of the Results should be summarized in Tables. This would make a comparison of SGD sites much easier for the reader. The descriptive nature of this portion of the paper is very tedious to read. Also, section 2.5 "Water Chemistry" is a major constituent of this study yet it only pops up in the results section. This section should be expanded and better introduced in the beginning of the manuscript. It is not clear to me how section 3.1 or Fig. 5 or 6. explain the "conditional nature" of each spot. Please expand and explain more clearly.

We agree with the reviewer and expanded the section of water chemistry including an adequate introduction to make it clearer.

We also added a table summarizing the results to gain more clarity.

Concerning the "conditional nature", we believe we may have evoked a misunderstanding. The term "conditionally" in section 3.1 (p8L21) refers to the variance analysis and its limited expressiveness concerning specific temporal behaviour. The way the variance analysis is performed and presented provides a general view (over the entire analysed time period or the entire time stack) on temporal behaviour. Yet, the variance analysis prohibits insights in specific parts of the temporal period being analysed, say only the first half or even single temporal elements such as single images as in the presented case. This is why we wrote "conditional", as it cannot shed light on specific parts of the analysed period. To avoid confusion, we changed the sentence accordingly.

Are the number and quality of references appropriate?

The presented references are fine but a large body of work by the above mentioned reference should be included. On page 3 section 2.1 the authors mention that the site this study was done at was the site previously studied by others. It is important to summarize these previous studies and put your study in their context. Simply referencing does not suffice in this case.

We changed the passage and tried to put our study in a proper context.

Is the amount and quality of supplementary material appropriate?

Yes.

AGAIN, I want to make clear that I find this manuscript extremely valuable despite some significant language and syntax problems.

Thank you, we really appreciate your evaluation and want to thank you again for your efforts, time and passion spent to help us improve our manuscript.

Reply to Reviewer 2:

We want to thank Reviewer 2 for the thoughtful contributions and comments to our manuscript that underline the careful reading for which we are really grateful. In the following we will comment on a point-by-point basis on the given comments (reviewers comments are given in bold and answers are given in italic).

ABSTRACT:

The use of in-situ in the abstract made me think that you were making in-situ measurements, but such measurements are not adequately presented and used in the paper.

The use of "in-situ" is used in the abstract during the introduction sentences, which puts the study in its general semantic context. Nevertheless, previously obtained in-situ data concerning SGD and spring water samples are mentioned as well throughout the manuscript. In our understanding the latter is used and presented adequately. However, we reworked some of the passages concerning obtained in-situ data to improve its presentation.

Page 1 Line 2 - "...measurements may provide" - not all in situ measurements are made to determine continuous temporal changes as implied by the sentence.

We agree. The statement was too general. Thus, we changed the text according to the reviewer's suggestion.

INTRODUCTION:

Page 2 Line 21 – can reference Tamborski papers and Kelly papers.

One paper of Tamborski and Kelly was added as reference.

MATERIALS AND METHODS:

Why is there no materials and methods text below the 2 heading on page 3 and then a duplicate heading of 2 Material and Methods on page 7 with lots of text below it that looks more like results?

To our best knowledge, there is no need to have text below main headings. However, we reorganized the text and separated "study area" and "material and method" in individual sections. The separation leads the general alternation of heading and text. In regard to the duplicate heading and a partial numbering chaos, we agree to the reviewer. During the conversion to the HESS format, we must have caused the chaotic conditions that we will correct in the revised version and double-check prior to resubmission.

Also, I think Tamborski should be referenced within the section 2 text starting on page 7.

We added the reference: Tamborski, J. J., Rogers, A. D., Bokuniewicz, H. J., Cochran, J. K., and Young, C. R.: Identification and quantification of diffuse fresh submarine groundwater discharge via airborne thermal infrared remote sensing, Remote Sensing of Environment, 171, 202-217, 2015

In general, the methods section could benefit from more references and better explanation of software packages and processes used.

We agree, in the manuscripts current state, it is hard to reproduce the method. In the revised manuscript, we brought in more clarity, and additionally we included an offer to distribute the code written in Matlab to any researcher upon request.

Section 2.1 is a one sentence paragraph that was lacking in critical information about the study area. At the very least, please add information about the number of known springs in the study area and perhaps the volume of water they discharge. Is there seasonality to the discharge volumes?

Information on number of springs is indirectly given in Figure 1. We decided against giving absolute numbers in the text out of several reasons.

1. *During the last years, we repeatedly observed several locations along the western coast and recognised a highly dynamic system of coming and leaving springs, on- and offshore.*
2. *We found and investigated the 8 submarine springs given in Figure 1 and a lot more in the near vicinity, but this number is only a fraction of focused submarine springs in the wider area, not to speak of the entire coastline that we are not able to tell.*
3. *It is unclear how long springs (both terrestrial and submarine) exist in the investigated area, due to the observed continuously changing groundwater flow systems, as a consequence of changing hydraulic gradients due to the falling Dead Sea and the associated groundwater levels and the heterogeneity of the sedimentary body, acting as aquifer.*

Thus, giving an absolute number would be valid for the moment and the area of investigation, but certainly not in general terms.

Section 2.1.1 the last sentence proposes a connection between groundwater discharge and the maturity of the karst system. It seems like this is the hypothesis that is set out to be tested in the paper, but the authors never come back to this thought in the discussion or conclusion sections.

It is not really a hypothesis to be tested, since we cannot really test it. We merely proposed one possible and very likely explanation, resulting from the observation of burst-like discharge events from diffuse springs in the thermal infrared data. The proposed explanation (maturity of the karst system) presented, which is certainly not the final one, is already introduced in the section "hydrogeological section" and also linked to the discussion and conclusion sections, e.g. p13L 22f "[…] Discharge behaviour in this case depends on the maturity and geometric formation of the conduit network, is therefore highly anisotropic, heterogeneous, and features a rapid flow (Surić et al., 2015) […]" or p14L32ff "[…] And lastly we are able to reveal a short-term periodicity in the order of 20 to 78 seconds for diffuse SGD which we attribute to an interplay of conduit maturity/geometry and wave setup […].

Section 2.1.2 I don't consider diffuse flow to be onshore springs, but the title of the section says that there are onshore springs. What and where are the onshore springs that are meant to be described in this section? This becomes very important for understand the information presented in section 2.5

Neither do we consider onshore springs to be explicitly diffuse in discharge, nor does the heading state it. Instead the heading reads as "Submarine groundwater discharge and onshore spring characteristics". Yet, we agree that the formulation, particularly in the last paragraph, can cause the impression that onshore springs are occurring as diffuse springs. Thus, we changed that passage, describing onshore springs characteristics separately and referring to Fig. 1d in which the spring-locations are shown.

Section 2.1.3 What about ambient warming of shallow areas compared to deeper areas? How do you address this issue? It seems like your data may have been collected at night. If so, say so.

First, we need to express our sincere gratitude to reviewer 2 who pinpointed at a typo with severe understanding-consequences. Although we state the investigation time to be 12:43 a.m., we meant to write 12:43 ***p.m****. Thus, it was not*

during night, which would not be allowed, but during noon. We changed it accordingly. Second, shallow areas are certainly more warmed compared to deeper areas with more incoming radiation. Yet, since we do not investigate absolute SSTs but the SST variability of a time span of less than 3minutes, this fact is not of relevance. It would be of relevance, if we would compare data covering a longer time span, say for a day, during which the warming would play a major role, but for three minutes the warming effect is certainly negligible.

Page 5 Line 1 With data acquisition between what times? Your UAV was airborne between 12:43 and 12:50 AM, but when were the data actually collected. You present fewer minutes of data than advertised here.

With time needed for take-off and landing, the actual recording time is from 12:45 to 12:48 pm. We added the recording time in the revised version of the manuscript.

Figure 2 is not necessary because the text adequately describes what the authors did

Quite frankly, although we somewhat agree with reviewer, who apparently is from the field of remote sensing and thus familiar with camera characteristics, we still think it is beneficial to keep Fig. 2 especially for readers with a non-remote sensing background. The figure shows nicely in how far frames relate to recording time and what is meant with master and slave images.

What program did you use to co-register your images?

All image processing steps (co-registering, cropping, extraction of focused and diffuse SGD, spatiotemporal analysis) were conducted within Matlab. We added the software to the section and tried to refine the description regarding the image processing as it was also noted by Reviewer 1 that this section is not reproducible. Since the processing requires knowledge on image processing, which some research may not possess, we also offer to distribute the Matlab code upon request in the revised version of the manuscript.

Why did you choose 150 pixels? I have seen very small-sized focused SGD flows (much smaller than 150 pixels) and very large focused SGD flows.

The threshold of 150 is subjective with the aim to focus on larger patterns only. Admittedly, smaller areas (<150 pixels as connected area) which also fulfil the temperature variance criterion of being smaller than 0.019 do also exist. Yet, all of these areas are due to stones that were not masked especially close to the shoreline. Other areas which might provoke the assumption of being below the variance threshold of 0.019 are in fact above 0.025 and thus, do not reflect focused SGD.

Page 6 Lines 18-19 I'm confused about using frame 210, which you say is not shown, and then reference the first image in Figure 3 later on in the same sentence. I don't understand what is happening here.

We agree that it is a bit confusing. Frame 210 showed the clearest picture with the largest extent of thermal anomaly caused by diffuse SGD and was therefore chosen to determine the transect length. Although comparable, the visible anomaly extents shown in frame 1 are smaller, but already indicate the general anomaly/discharge picture. Therefore and due to its position as first frame, the first frame was chosen to be shown instead of frame 210. To ease the reading and understanding, we changed the lines which reads now: "As a consequence we delineate diffuse SGD from a single frame (frame 210 – not shown) in which thermal radiation patterns and maximum spatial extents induced by high discharge rates are unequivocally detectable (a comparable single image is shown in Fig. 3-upper left image)."

What software did you use to do the inverse modelling?

The inverse modelling was pursued with Phreeqc 3.2 applying thermodynamic database Pitzer.dat. Although already included, we rewrote the passage to make it clear.

Page 6 Line 26 – you say single SGDs, are these point source or diffuse or both?

At locations where it is not specifically stated as diffuse or focused SGD both are meant. As the reviewers' questions points at an unclear statement, we clarified it.

Section 2 (with text) Does the last sentence of the last paragraph of the section refer to known spring locations? Can these be provided in one of the figures or referenced in the sentence?

Yes, they refer to the known springs (focused SGD and onshore) as you need in-situ water samples to apply the inverse modelling. All spring characteristics included in the modelling are given in Table 2 and spring locations are shown in Fig. 1. We added references at appropriate positons in the text.

RESULTS:

Section 3.1 What assumptions did you make to arrive at the statement "we expect here the most pristine patterns representative for each spot"?

The assumption behind relates to the interplay of active forces, or more specific, the discharge momentum vs. any external influence such as waves, currents etc. Only at the maximum extent, we assume the external influence to be lowest compared to any other location along the thermal anomaly. Thus, here we can observe anomaly patterns best which reflect temporal SGD behaviour with least external influence.

Section 3.1.1 does the 1st focused SGD spot correspond to one of the springs labelled in Figure 1? If so, please say so in the sentence. Same thing for the 2nd and 3rd focused SGD spots.

Yes, it does and is revealed in the result section p8L2ff and p8L10ff. However, we added the corresponding sampled spring numbers in section 3.1.1.

Section 3.1.2 Where are the diffuse SGD spots relative to Figure 1? I don't typically think of diffuse SGD as being a "spot-like" and circular feature; rather, diffuse SGD is typically patchy and spread out over fairly large areas that do not have to be circular features. Perhaps diffuse SGD locations may be better than diffuse SGD spots?

We too thought diffuse SGD to be patchy and observed it in the same way in the field due to the development of schlieren. Based on the patchy and areal observation we show diffuse SGD as area in Figure 1 instead of discrete symbols. The area is 20-25m long as described in section 2.1.2. However, in the present case, the two forms, diffuse and spot-like or focussed discharge, seem to co-exist in the same area. TIR images confirm the observation showing elevated and patchy SSTs in that area along the coastline. Yet, TIR images also reveal spot like discharge within the diffuse SGD area, evoking a CVP (counter rotating vortex pair) and thus suggesting a lateral, pulse-like discharge at the coastline (in contrast to SGD emergence at the sea bottom which induces a buoyancy driven vertical ascend of SGD-water and as a consequence circular pattern on the sea surface). Thus, we all should possible change our spatial thinking in the way as to think of SGD either in the form of focused or diffuse but to consider a possible spatial co-existence of both forms at the same spot/location.

Section 3.2 What does temporally mostly pristine mean? What software was used for the temporal autocorrelation analysis?

"Temporally pristine" means that the true temporal signal of SGD will be most pronounced in the centre (focused SGD) or at the midpoint of the transect (diffuse SGD). In other locations the temporal behaviour will be more influenced by external

influences such as waves or currents. The autocorrelation analysis was conducted using Matlab. The latter fact is now included in the revised version of the manuscript.

Section 3.2.2 Why reference Figure 4 in line 18? Also what does "ones" refer to in line 20 and in line 24?

Reference to Fig. 4 is irrelevant and was deleted. The "ones" refer to SGD spots (the first "ones" to diffuse SGD spots 1 and 2 and the second "ones" to all diffuse SGD spots). To increase clarity, both "ones" were exchanged with the respective naming of the SGD spots.

Section 4.1 Line 15 the 3rd SGD spot refers to focused, SGD, correct? If so, why does the very next sentence starting with "This" refer to diffuse SGD? What is "This" referring to? There is an awkward transition here. Also, why reference Figure 4 in a sentence that talks about diffuse SGD?

Correct, but the reviewer seems to miss the context. In the indicated passage we talk about the shape of the SGD patterns and possible causes. In all three focused SGD cases the shape is elliptic and northward oriented, which is more pronounced for the 1st compared to the 2nd and 3rd focused SGD spot. We hypothesise the cause for shape and the deflection trend to be the diffuse discharge or the discharge momentum induced by the burst-like discharge events from, diffuse SGD. The "this" refers to the deflection. The reference to Fig. 4 is wrong and should refer to Fig. 3. We clarified the "this"-misunderstanding and the wrong reference in the revised version.

Section 4.2 would benefit from referencing a figure: The variance image (Figure ?) provides...

We agree and added several figure references to Section 4.2.

I'm also not convinced that the higher discharge rates reveal karst conduits (if higher discharge rates is what "it" refers to) close to the shoreline. We know that faults, fractures, paleochannels, and animal burrows can also be conduits of groundwater
flow. Just because the area has karst, doesn't mean that karst is the only explanation for the flow patterns. Please justify your assumption of karst conduits more fully. Are you relying on your insitu data? If so, cite it as support in this section.

We reworked the final statements. While paleo-channels are unlikely in the studied part of the sedimentary fan of Wadi Darga as sedimentary conditions derived from close-by drillings suggest, animal burrows can be excluded for the present case as well, as the sedimentary body we are discussing is soaked with brine, and thus at least as saline as the Dead Sea, making it difficult for any macrozoobenthos or larger animal to survive.
On the contrary, faults may play a role in the present setting. Former investigations by Ionescu et al. (2012) show that microbiologically accelerated dissolution of hosted minerals in the sedimentary body occur widely. We assume, fractures and faults, maybe the result of neotectonic activities may form the initial pathways for water flowing eastwards to the Dead Sea and will be widened (in terms of hydraulic aperture) by dissolution.

Section 4.3 Why keep referencing figure 4 throughout this section? Figure 3 The red writing on the figure is very hard to see and read.

The referencing appears to remain from an earlier version of the manuscript and was not correct before the first submission. Thank you for the lead, we changed it in the revised version. Likewise, we changed the red lettering in Fig. 3.

Figure 4 If these spots correspond to spring numbers in Figure 1, please add spring numbers here. It seems like you should be able to do a very rough calculation of the volume of water coming from the springs since you know the water column depth and the size of the surface expression of the thermal plume. Do you have estimates for the volume of water issuing from these springs and how does that volume compare to a rough calculation?

We added the spring number below the graphic as suggested. Concerning the volume calculation, to our best knowledge there is no approach calculating the volume of water or the discharge rate, based on depth and surface area nor is there any measured discharge rate/volume available for the investigated focused SGDs. We believe the reviewer thinks of a conus as first approximation of the SGD plume beneath the water surface, using known principles to calculate the volume of the cone/water plume beneath the surface.
Although generally correct, the cone approximation has severe flaws and eventually would not provide any more insight to potential volume/rates deriving from SGD as the simple areal surface expression (For all three focussed SGDs: Area [m²]: 15 / 28 / 4 - Volume [m³]: 71 / 210 / 19).
The SGD plume within the water column is not at all a conus as both theoretical (see works of Jirka et al. or Papanicolaou et al.) and own experimental (not published) works proof. Instead it is rather tube-like in the bottom near area and develops a pronounced funnel near the water surface. The ratio between tube and funnel depends on a diversity of factors including density and temperature gradients, entrainment and momentum (some of factors are even interdependent, making it difficult to determine the dominant factor). Further unknown is the entrainment of ambient water and thus the amount of pure SGD water within a defined water parcel. Thus, when calculating the volume using the conus approximation would give us the volume of water (both SGD and ambient water) within the conus but certainly not a SGD volume. To determine the SGD ratios using the presented approach we currently plan a further experiment along with further in-situ measurements but this is not yet pursued and thus not presented.

Figure 5 should add NTR to middle column so reader is reminded of acronym in text. The read writing in the first column is very hard to read. The caption says red boxes in figure 4, but there are no red boxes in figure 4.

We added the NTR acronym in the caption of figure 5 and 6 to make it easier for the reader to follow and changed the red lettering to facilitate readability. The red boxes are contained in Fig. 3. We corrected the wrong reference.

Figure 6 should add NTR to middle column so reader is reminded of acronym in text. What is the third transect pixel? Is that pixel 3 of the transect, closest to shore?

Concerning NTR, see comment before. The third pixel of the transect is close to the shore. We added a respective statement in brackets in the figure caption.

Table 1 are the peak values statistically different than the non-peak values. It would be very beneficial to do a simple statistical analysis to demonstrate significance.

We will add the test and its results in the revised version.

Table 2 is illegible

We agree and we will change it in the revised version.

List of relevant changes

- Inclusion of references from the Near-Shore community (reviewer 1) concerning data processing and of relevant references underlining the applied methodology (reviewer 2)
- Reworked the entire method section to introduce more clarity on the applied methodology (mostly image registration) (reviewer 2)
- Included the offer of distributing the Matlab code created and used for the manuscript (reviewer 2)
- Reworked the interpretation and conclusion concerning the effects of Karst geometry on the pulsating behaviour of diffuse springs, the effect of bathymetry, and approach transferability (both reviewers)
- Included a subsection of the discussion entitled with "Potentials, limitations and potential errors" (reviewer 1)
- Conductance of proofreading by a professional proofreader with scientific background (Paul Ronning - www.ronningtranslation.com) (reviewer 1)
- Corrected the erroneous numbering in the heading (both reviewers)
- Included a table in the result section that summarizes the main findings (reviewer 1)
- Introduced the hydrochemistry part earlier and expanded it (reviewer 1)
- Corrected semantically unclear parts of the manuscript (reviewer 2)
- Improved Figures according to suggestions (reviewer 2)
- Added a statistical analysis demonstrating the statistical difference between peak and non-peak values (reviewer 2)

Combining continuous spatial and temporal scales for SGD investigations using UAV-based thermal infrared measurements

Ulf Mallast[1], Christian Siebert[1]
[1] Helmholtz Centre for Environmental Research -UFZ, T. Lieser Str. 4, Halle 06120, Germany
Correspondence to: Ulf Mallast (ulf.mallast@ufz.de)

Abstract. Submarine groundwater discharge (SGD) is highly variable in spatial and temporal terms due to the interplay of several terrestrial and marine processes. While discrete in-situ measurements may provide a continuous temporal scale to investigate underlying processes and thus ~~accounts~~account for temporal heterogeneity, remotely sensed thermal infrared radiation sheds light on the spatial heterogeneity as it provides a continuous spatial scale.

Here we report results of the combination of both~~,~~ the continuous spatial and temporal scales, using the ability of an Unmanned Aerial Vehicle (UAV) to hover above a predefined location, and the continuous recording of thermal radiation of a coastal area at the Dead Sea (Israel). With a flight altitude of ~~65m~~65 m above the water surface resulting in a spatial resolution of ~~13cm~~13 cm and a thermal camera (FLIRTau2) ~~which~~that measures the upwelling long-wave infrared radiation at ~~4Hz~~4 Hz resolution, we are able to generate a time ~~sequence~~series of thermal radiation images ~~which~~that allows us to analyse spatiotemporal SGD dynamics.

In turn, ~~we are able to enhance~~ focused SGD spots, otherwise being camouflaged by strong lateral flow dynamics, are revealed that may not be observed on single thermal radiation images. ~~Plus, we show the~~The spatiotemporal behaviour of ~~a~~an SGD induced thermal radiation pattern ~~to vary~~varies in size and over time by up to ~~55~~155% for focused SGDs and by up to 600% for diffuse SGDs due to different underlying flow dynamics. These flow dynamics even display a short-term periodicity in the order of 20 to 78 ~~seconds~~sec for diffuse SGD, which we attribute to an interplay ~~of~~between conduit maturity/geometry and wave setup.

1 Introduction

Submarine groundwater discharge (SGD) is defined as "any and all flow of water on continental margins from the seabed to the coastal ocean" (Burnett et al., 2003). The definition already implies several ~~shares~~proportions of water with different ~~origin~~origins contributing to SGD. ~~Next to~~Apart from recirculated seawater, it is also fresh groundwater of meteoric origin. The relative share of each water contribution depends on terrestrial and marine controls. Recharge amounts, aquifer permeability and hydraulic gradients define the terrestrial groundwater contribution, which may be the ~~mayor~~major SGD share in areas with high permeability, such as karstic environments. In areas with low hydraulic gradients and low aquifer permeability~~ the mayor SGD share shifts towards~~, recirculated seawater ~~driven~~as a share of SGD predominates. The recirculation is induced by ~~constantly changing~~the highly variable hydraulic gradients ~~that are~~ caused by tidal or lunar cycles, storms, or wave setup. In-situ measurements such as seepage meters, multilevel ~~piezometer~~piezometers, tracers, etc~~.~~.,

possess the ability to discriminate between the SGD shares and allow a linkage to the underlying processes, since the investigated temporal scale is continuous and ranges between daily to seasonal cycles (Taniguchi et al., 2003a; Michael et al., 2011). Yet, all of this cannot account for the spatial variability, as the entity and interaction of terrestrial and marine controls lead to a highly variable SGD appearance in terms of discharge type (diffuse vs. focused), temporal discharge behaviour, flow rates, spatial abundance (even over small spatial scales), and mixing~~, and of its temporal behaviour~~ (Michael et al., 2003; Taniguchi et al., 2003b; Burnett et al., 2006).

In contrast, remote sensing technology allows ~~identifying~~identification and ~~quantifying~~quantification of SGD over larger spatial scales without neglecting its spatial and ~~partly even~~ temporal variance, or the need to extrapolate from in-situ measurements. Depending on the intended spatial scale, utilized platforms differ between satellite (spatial coverage >10~~.000km~~,000 km²), airplane (spatial coverage >~~100km~~100 km²), and ~~lately~~ unmanned aerial vehicle (hereafter UAV) systems (spatial coverage >0.~~1km~~1 km²). From these systems the majority of all approaches measure thermal infrared radiation (hereafter thermal radiation/radiances) (i.a.~~o.~~ Mejías et al., 2012; Kelly et al., 2013; Mallast et al., 2013b; Schubert et al., 2014; Lee et al., 2016).

The principle of using thermal radiation for SGD detection is based on temperature contrasts between SGD water and ambient water at the sea~~-~~ surface. ~~These~~Since the surface temperatures are directly proportional to emitted thermal radiation (see Stefan-Boltzman Law) and ~~assuming~~assume a rather similar emissivity for water~~), why thermal sensors allow identifying SGD through~~, sea surface temperature contrasts evoke distinguishable thermal radiation patterns or thermal radiation anomalies~~.~~, which are indicative of SGD.~~ This qualitative approach ~~is~~has been expanded by a few studies that use thermal anomalies to quantify SGD through a relation of anomaly (plume) size to measured or modelled SGD rates (Kelly et al., 2013; Tamborski et al., 2015; Lee et al., 2016). Given a positive buoyancy of less saline groundwater in marine environments, the intriguing simplicity of these approaches is based on the momentum of discharging groundwater (Mallast et al., 2013a) and a potential deflection in the water body due to currents / wave action (Lee et al., 2016) or external forces (e.g. wind) (Lewandowski et al., 2013), and Newton's law of cooling (Vollmer, 2009). While the latter leads to a convective heat transfer between the discharging and the ambient water with ~~an~~ exponential adaption behaviour at the fringe of the plume, the momentum and deflections are the forces defining the size and shape of the plume. In turn, ~~it~~the momentum leads to a positive relationship between plume size and discharge rate (Johnson et al., 2008; Mallast et al., 2013a; Lee et al., 2016) for parts of the plume not being deflected~~. Albeit~~ and demonstrates the ~~thoroughly clear~~ practicability and numerous advantages in terms of spatial continuity ~~and as a~~. The possible quantification approach~~, all studies rely~~ however, relies on thermal radiation snapshots recorded at a certain instantaneous time~~.~~ (Kelly et al., 2013; Tamborski et al., 2015).

Thus, in terms of scale, the advantage of remote sensing for SGD investigations is ~~clearly~~ the continuous spatial scale, which allows ~~deriving~~ the derivation of a ~~clear~~general picture ~~of~~in regard to SGD abundance and quantity independent of its

appearance and spatial variability. On the ~~contrary~~other hand, the advantage of in-situ measurements is explicitly the continuous temporal scale permitting a process understanding and ~~elaborating~~elaboration on the drivers.

However, with the advent ~~of UAVs~~ and the ability of multi-copters as a type of ~~UAVs~~UAV to hover over a predefined location, it becomes ~~possibly~~possible to combine the continuous spatial and temporal scales~~. Consequentially the combination offers~~ in an unrivalled resolution and to investigate the spatiotemporal behaviour of SGD in ~~a~~one context ~~and with a spatial and temporal resolution that was not possible before~~. Here we report the results of such a study that uses a thermal camera system mounted beneath a multi-copter ~~hovering~~. The multi-copter hovers above a predefined location to i) investigate the spatiotemporal variability of focused and diffuse SGD and ii) to outline additional values of the presented approach. The study is conducted at a site ~~of~~on the hypersaline Dead Sea, at which previously investigated submarine and terrestrial springs emerge. Existing hydraulic gradients in the discharging aquifers and high density differences between ground- and lake water qualify the terminology SGD, which is usually bound to marine environments only.

~~2 Material and Methods~~

2~~.1~~ Study area

The study was conducted at a known and pre-investigated SGD site (~~Ionescu et al., 2012; Mallast et al., 2013b; Siebert et al., 2014~~see section 2.2) at the ~~eastward side~~eastern slope of the sedimentary fan of Wadi Darga, located at the western coast of the Dead Sea (Fig. 1a, 1d and 1e).

2~~.1~~.1 Hydrogeological setting

Discharging groundwater at the study area is replenished in the Judean Mountains either through precipitation or ~~flashfloods, which enter~~flash floods that infiltrate into the Upper Cretaceous lime- and ~~dolostone~~ dolostones of the Judea Group Aquifers (JGA) and flow ~~eastwards~~east towards the Dead Sea ~~Transform (DST). The~~ Rift (DSR). After passing the transition to the ~~DST~~DSR, which is marked by normal faults and block tectonics~~. Within the Graben,~~, fresh groundwater enters the Quaternary fluvio-lacustrine Dead Sea Group (DSG) that is deposited in front of the Cretaceous rocks (Yechieli et al., 2010~~) and receives fresh groundwater through lateral flow from the JGA.~~). The DSG consists of ~~clastic sediments (gravel and sand) and~~ stratified fine-grained lacustrine sediments (clay minerals, aragonite, gypsum, halite~~) (~~), which are intercalated with coarser clastic layers. At wadi outlets, the lacustrine strata are displaced with fluviatile fine- to coarse clastic sediments (Yechieli et al., 1995). ~~Groundwater flow occurs through several subaquifers with different groundwater levels and chemical compositions due to~~

Due to the alternations of coarse and fine strata~~–~~, groundwater flow occurs through separated subaquifers that possess different groundwater level (Yechieli et al., 2010). In addition, ~~due to the high solubility of~~ preferential flow paths in the form of dissolution tubes and cavities develop due to dissolution of the evaporitic minerals ~~and microbial activity, dissolution cavities develop, representing zones of higher hydraulic conductivity and thus preferential flowpaths. They lead to a karst like behaviour of groundwater movement~~ (Magal et al., 2010; Ionescu et al., 2012). ~~However, due to the~~ The dissolution process accelerates with the continuous and fast drop of the Dead Sea water level of ~1~~.3m~~ m per year, which forces the ~~entire~~formation of new groundwater flow ~~system is highly dynamic~~paths. The resulting~~ in different degrees of maturity of its~~, partially karstic ~~parts. As a result,~~ flow system in the DSG is highly transient, resulting in immensely variable discharge rates, discharge locations and chemical composition of springs along the ~~lake shore vary intensely~~lakeshore (Burg et al., 2016). ~~It is hence proposed~~Besides admixing of interstitial brines to the groundwater, the degree of water/rock interaction in the DSG controls the groundwater's composition. Hence, observable ~~highly variable chemical compositions~~large differences in the composition of discharging groundwater, which occur even within ~~meters~~the range of a few metres, are an expression of the heterogeneous maturity of the karst system. The less mature the conduits are~~,~~ the larger is the ratio between wetted ~~surface~~soluble surfaces and volume~~, resulting in highly variable concentrations between~~. Consequently, diffuse SGD exhibits a high load of dissolved solids and thus is saline (less mature karst system~~) and~~), while focused SGD is less loaded and exhibits a lower salinity (mature karst system).

2.~~1~~.2 Submarine groundwater discharge and onshore spring characteristics

~~At the investigation site, focused SGD occurrences were mapped in 2011 and 2012 by SCUBA divers and hydrochemically investigated. Based on their findings groundwater emerges from mature karst like underground~~ cavities down to depths of ~~30m~~30 m below ~~water table~~sea surface (Ionescu et al., 2012; Mallast et al., 2014).

From these cavities groundwater emerges as focused SGD. Subsequently, density differences between SGD water (1.00–1.~~19g~~19 g·cm^{-3}) and Dead Sea brine (1.~~234g~~234 g·cm^{-3}) trigger a continuous positive buoyancy (buoyant jet) of the emerging groundwater towards the ~~lakes sea~~lake's surface. Within the water column and alongside the buoyant jet ~~develop,~~ considerable turbulences develop, entraining ambient Dead Sea ~~water~~brine. Thus, the ascending water represents a mixture of fresh ~~and~~to brackish ~~water.~~groundwater and lake brine. Once the ascending ~~water~~mixture reaches the ~~lakes sea~~lake's surface, it develops a radially orientated flow away from its jet centre causing a circular-like pattern. These patterns are ~~partly~~partially visually observable as shown in Mallast et al. (2014) at the Dead Sea ~~or~~and in various other cases (Swarzenski et al., 2001).

Apart from focused SGD, diffuse SGD occurs at the investigation site as well, either in various depths below water surface (Ionescu et al., 2012) or at the shoreline. At the study area one diffuse SGD site exists directly at the shoreline (Fig. 1e). The discharge seems to occur over a length of approximately 20-~~25m parallel to the shoreline~~25 m alongshore and was only detectable visually through the occurrence of schlieren in the lake brine. ~~Sampling of this water was not possible as neither the true origin nor any~~ However, low discharge ~~was identifiable~~rates in combination with the immediate mixing with the lake brine impede any attempt to sample that ~~was unaffected by seawater. However, five more springs exist onshore that have been sampled~~water.

~~**2.1.3 Hydrologic and atmospheric setting**~~

At the time of emergenceIn order to still be able to compare groundwater characteristics, we sampled five onshore springs (Fig. 1d). All are in close proximity to previously mentioned SGD and to the shoreline, but emerge as focused flow in different elevations of 0.5-10 m above the Dead Sea water level. The water characteristics are shown in Table 2.

2.3 Hydrologic and atmospheric setting

~~According to on site measurements,~~ SGD water temperatures at the orifices are 21-31.5°C. During the time of investigation the Dead Sea had a skin temperature of ~21°C providing a temperature maximum difference of 10.5°C between ~~warmer~~ groundwater and ~~cooler~~ ambient Dead Sea ~~water~~brine. Wind speeds amounted to 0.~~87m~~87 m·s^{-1} (±0.16) approaching from

SE to E (80°-128°). Occurring waves, which may influence SGD size and shape, had a frequency of 3-7 ~~seconds~~sec with estimated wave heights <~~15cm~~15 cm. During the flight, cloud free conditions and thus ~~homogenous~~homogeneous solar radiation existed ~~being,~~ equally reflected at the sea~~-~~ surface ~~within~~throughout the entire ~~recorded~~covered area.

~~2.2 Material~~

3. Materials and Methods

The general approach to investigate the spatiotemporal thermal radiation variability induced by SGD ~~consist~~consists of hovering with an UAV (~~multicopter~~multi-copter - model: geo-X8000) above a pre-defined SGD spot (Fig. 1c) over a time period of several minutes. The flight was conducted on 10 Feb~~., 10th~~ 2016 between 12:43 and 12:~~50 a.m.~~50pm, with activated image recording between 12:45 to 12:48pm. During that flight the UAV ~~is~~was equipped with a thermal system comprising i) a long-wave infrared camera core (FlirTau2), which is an uncooled VOx Microbolometer with a ~~19mm~~19 mm lens and a 640x512 focal plane array (FLIR® Systems (2016)) and ii) a ThermalCapture ~~module~~ radiometry module and image grabber (TeAx Technology, 2016~~)).~~). The system senses ~~LWIR~~long-wavelength infrared radiation in the spectral range of 7.5~~-~~13.~~5µm~~5 µm with a sensitivity of <~~50mK and captures LWIR (thermal)~~50 mK. Subsequently, sensed radiation is captured as 14~~-~~bit images at a frame rate of ~~9Hz~~9 Hz, from which only every ~~5th~~fifth frame is exportable (approx. 4~~-5Hz)~~5 Hz), deduced after our own tests. The core was calibrated prior to the flight using an internal flat-field-corrector.

The hovering position ~~is~~was at 31.576516N/35.415775E with a flight altitude of ~~65m~~65 m above Dead Sea level. Due to the GPS controlled nature of the UAV, the hovering position displays a certain spatial variability which is according to the flight log ±1.~~5m~~5 m in horizontal dimension and ±1.~~75m~~75 m in vertical dimension. Position and altitude ~~are~~were chosen ~~(~~i) ~~due~~according to Israeli regulatory framework and ii) to cover land and water in equal shares. The latter ~~is~~was important for the ~~co-~~image registration of each recorded image to a selected ~~master~~reference image (see section 2.3) in order to correct the spatial variability of the UAV and the sensor during hovering, and to determine the position accuracy of the ~~co-~~image registration, which ~~is~~was based on two aluminium reflectors placed directly on the shore (Fig. 1b and 1c).

~~2.~~3.1 Data processing

Thermal radiance image recording with 4-5 Hz results in a total of 670 images recorded within a time span of 167 ~~seconds~~sec. Each image displays thermal radiances emitted by the surface. According to the Stefan-Boltzman Law these radiances are directly proportional to the existing surface temperatures and thus are the basis for the present study. Yet, due to the UAV position variability while hovering above the pre-defined flight position, the mapped image footprint is not congruent for each image but varies spatially ~~in~~at the same magnitude as the position variability~~.~~, which is also described in Holman et al. (2011).

To overcome the varying footprint, we define the first image of the set as ~~master~~reference image and all remaining ones as ~~slave~~input images (Fig. 2). Subsequently all ~~slave~~input images are automatically co-registered onto the ~~master~~reference image using an intensity based image registration~~.~~ within a Matlab 2016 environment[1]. The applied image registration uses a similarity transformation ~~which~~that considers translation, rotation and scaling as possible factors induced by the UAV position variability and thus the non-congruent image footprints. It was chosen due to the ~~facts~~fact that the short-time differences between images ~~will~~would not cause i) nonlinear geometric differences ~~while especially~~ nor ii) a change of intensities, which in the present case, are radiances. Instead, the land and placed reflectors especially represent those rigid parts with similar intensities needed ~~to calculate a reliable transformation~~for intensity based image registration (Kim and Fessler, 2004).

~~The core of the~~ intensity based image registration consists of comparing an input matrix~~. The matrix similarity between input matrix (master~~ (reference image) ~~and~~with a transformation matrix (each ~~slave image) is determined using a mean square metric that was iteratively optimized through a~~input image). During an iterative regular step gradient descent optimization, the transformation matrix is transformed incorporating scaling, rotation and translation. The intensities of both, the input and transformation matrices, are compared using a similarity measure (e.g. a mean square metric as in the presented study) with the aim to maximize the similarity between both matrices (Viana et al., 2015). The iterative optimization process continues until ~~a minimum step length of 1e-05 was reached.~~ the maximum iteration criterion reaches 1000 iterations, or the optimization criterion reaches a Maximum Step Length of $1.0e^{-2}$. This just described image registration process is repeated for all input images.

The so obtained co-registration To provide a further independent accuracy ~~of all images, evaluated based on~~measure, we use the two previously described aluminium reflectors. Similar to the automatic approach described in Holman et al. (2017) to find GPS targets, we define search windows in the registered input images, looking for the lowest radiance values (=reflector plates). Since the plates represent an area of several connected pixels, we then extract the mass centre of both plates and each image. Comparing the positions of ~~both reflectors, has a~~the mass centres of both reflectors in the reference image with each input image yields an independent spatial accuracy measure. The so obtained spatial accuracy of the image registration results in an RMSE of 0.58 pixel (1 pixel = 13 cm~~) with~~), a mean of 0.5 pixel, and a standard deviation of 0.3 pixel (see attachment Fig. S 1).

As a consequence of the ~~co~~ image registration process and the transformation of the input matrices, the footprint (covered area) varies. In order to be able to analyse the same covered area, we ~~reduced~~reduce the image sizes to a common footprint extent represented by all images. The so obtained image size amounts to 561x376 ~~pixel which are used during subsequent steps.~~pixels. Onto all co-registered images, we then ~~applied~~apply a manually derived land mask ~~and normalized the~~, masking out any radiances from land parts. Subsequently, radiance values of the remaining water area is normalized using a z-score normalization to account for potential global solar radiation differences that may occur over the time of investigation and

[1] The Matlab code used for the present study can be distributed upon request.

would affect the result. The so~~-~~-obtained processed image set ~~consist~~consists of a 3D data cube (x, y, t) of 670 images (hereafter frames) resembling a total time period of ~~~~167 ~~seconds~~sec, and showing normalized sea surface radiances in x, y dimensions.

3.2.~~4~~ Delineation of diffuse and focused SGD spots

Since SGD at the investigated site consists of focused SGD occurring offshore and diffuse SGD occurring at the land-water interface, we ~~used~~use different approaches to extract relevant discharge spots separately to finally pursue the intended temporal investigations. Given the assumption of a thermally stabilized area over time induced by focused SGD (Mallast et al., 2013b; Siebert et al., 2014) we calculate the thermal variance per pixel of the ~~entire frame set.~~data cube's temporal dimension t using Matlab 2016. The resulting low variance areas represent focused SGD sites~~. These~~ with constant and intense discharge. To extract focused SGD sites ~~are extracted using~~, we apply a subjective variance threshold of <0.019~~. To~~ and eliminate extraction artefacts ~~we apply~~, using a morphological closing and deletion of objects smaller than 150 pixel to obtain the low variance area representing focused SGD sites only.

In contrast, the observed diffuse SGD site along the shoreline discharges less water with lower discharge rates and thus, has a smaller momentum, which inevitably leads to a smaller, thermally stabilized alongshore area (~10^1- 10^2 cm perpendicular to the coastline~~) along the shoreline that is thermally stabilized. Yet, although being~~). While thermally stabilized, several direct forces such as breaking waves and currents influence the same area and thus the resulting thermal radiation pattern on the sea surface. These factors lead to rather high variances compared to focused SGD flow. Unfortunately, a similar variance can be expected from ambient areas ~~likewise being~~ influenced by highly dynamic flow field induced by waves, currents and discharge. As a consequence, we delineate diffuse SGD from a single frame (frame 210 – not shown) in which thermal radiation patterns and maximum spatial extents induced by high discharge rates are ~~clearly~~unequivocally detectable (~~first~~a comparable single image is shown in Fig. 3~~). Analogously~~ upper left image). Analogous to the focused SGD sites, we ~~applied~~apply a subjective threshold of >2.5 (normalized radiation) to extract discharge induced thermal patterns and eliminate extraction artefacts using a morphological closing to clean extracted pattern objects, followed by the deletion of objects smaller than 150 pixel to focus on larger patterns only.

2.~~5~~3.3 Spatiotemporal analyses

The likewise conducted We conduct two forms of (spatio)temporal ~~analysis includes~~analyses: (i) a spatiotemporal analysis to identify spatial variability of both thermal radiance patterns induced by diffuse and focused SGD and (ii) a periodicity analysis to reveal possible reoccurring temporal discharge patterns~~ of single SGDs.~~. To explore the spatiotemporal behaviour ~~of diffuse~~, and ~~focused SGD spots~~within a Matlab 2016 environment, we construct transects across the maximum ~~extents~~extent of each extracted SGD spot, as we expect ~~here~~ the most pristine patterns there. Along each transect, normalized

thermal radiances per frame are extracted, filtered using a 1D 9th-order median filter to reduce the white noise portion, and finally plotted, highlighting the spatiotemporal behaviour for each spot.

For the periodicity analysis we use an autocorrelation function, which measures the self-similarity of a signal (Tzanetakis and Cook, 2002). If discharge occurs regularly, it causes a periodic signal, which is expressed as significant peak (above or below 95% confidence interval) in the autocorrelation function. ~~These investigations are pursued at specific single pixels, which are the respective midpoint of each transect as~~As we expect the ~~clearest and~~ most pristine discharge induced thermal pattern signals ~~at these locations,~~ for both SGD types at the midpoint of each transect, we pursue the periodicity analysis at the specific transect midpoint pixel for each of the transects.

2.~~5~~3.4 Water chemistry and inverse geochemical modelling

~~Physicochemical~~To draw conclusions about the karst maturity of the flow net that feeds on- and offshore springs, we investigate the type and intensity of groundwater/rock interaction at each spring based on their on-site and chemical parameters. Physicochemical on-site parameters (temperature, density, pH, electrical conductivity) of all the above mentioned focused SGD ~~but also~~as well as onshore springs ~~were~~(see Fig. 1d and 1e) are measured in the field using WTW 350i and Mettler Toledo density meter. The sampling procedure for ~~water~~groundwater samples ~~in order~~ to analyse major element concentrations ~~of the discharging waters followed~~follows the procedure described in detail in Ionescu et al. (2012). Generally, samples for anion and cation analyses ~~were~~are filtered (0.22 µm CA filters), separately filled in HDPE bottles and stored cool. Cation samples ~~were~~are immediately acidified and later analysed applying ICP-AES. Anions ~~were~~are analysed using ion chromatography and bicarbonate by Gran titration~~.~~ (see Table 2).

~~The individual water/rock interactions, which lead to the chemical composition of the respective groundwaters in the springs were~~, are inversely modelled applying Phreeqc and Pitzer thermodynamic database. ~~The~~We apply the latter ~~was applied since the sediment~~due to the high activities in the modelled environment, consisting of a sedimentary saline aquifer body ~~through which the fresh groundwaters migrate is~~, soaked with interstitial brine, which admixes to the fresh groundwater. ~~Reactive solid phases were selected on the base~~On the basis of the abundant easily soluble minerals (halite, aragonite and gypsum~~)~~), we select reactive solid phases in the sedimentary succession~~. Ion~~, enable ion exchange on clay minerals ~~was enabled. Modelling~~, and evaluated modelling results ~~were selected~~based on the ~~base of~~ probability and lowest sum of residuals.

~~2 Material and Methods~~

4 Results

It is a proven fact that SGD influences the sea surface temperature and thus the thermal radiances, and that it is ~~clearly~~thoroughly detectable given a sufficient temperature contrast between groundwater and sea/lake water ~~temperature~~

and a certain minimum discharge volume/ and -momentum (Johnson et al., 2008; Lee et al., 2016, Tamborski et al., 2015). Our results confirm this fact as diffuse SGD induces thermal radiance patterns with values >1 (higher temperatures) that ~~is clearly~~are visible in the ~~first frame (~~upper left panel of Fig. 3~~)~~ and spatially ~~coincides~~coincide with our field observations. Yet, the single thermal radiance image suggests the diffuse discharge ~~to occur~~occurs in two distinguishable patterns.

The first pattern is a coastal fringe of ~~35m~~35 m length and of ~~~~10 pixel (1.~~3m~~3 m) width, showing elevated normalized thermal radiance (NTR) values >1. This alongshore distribution ~~along the shoreline~~ exceeds the visual results of ca ~~20m~~20 m by a factor of ~~two~~1.5 and suggests a homogeneously distributed, low velocity and low rate discharge of warmer groundwater that ~~partly~~ emerges partially onshore and ~~partly~~partially directly at the water/land interface (~~1st frame~~upper left panel in Fig. 3).

The second, seemingly dominant pattern is characterized by NTR values >1, but in contrast to the first, it consists of distinctive counter-rotating vortex pair (CVP) flow structures (Cortelezzi and Karagozian, 2001), discernible based on the mushroom shape, with length axes between ~~~~20 to ~~~~46 pixel (2.~~6m~~ 6.~~0m~~ m-6.0 m). The cause appears to be a focused and lateral jet-like discharge at four locations (~~1st frame~~upper left panel in Fig. 3). Plumes, caused by both discharge forms, are subsequently deviated towards N-NE.

Focused SGD with an expected circular to ~~elliptic~~elliptical shape as ~~observations shown in~~observed by Mallast et al. (2014) and Swarzenski et al. (2001~~) suggest,~~), are not ~~clearly~~unequivocally visible from the single frame (one thermal radiance image) only. At the upper and ~~at the~~ left ~~end~~ends of the single frame (~~1st~~first frame in Fig. 3~~)~~), three half-circular patterns with NTR values between -0.6 and 0 foreshadow focused SGD spots, which coincide with in-situ observed and sampled focused SGD spots 11/120, 11/121 and 12/382. ~~Yet~~However, from the thermal radiation perspective ~~clear~~, spatial indications for more than these three SGD-sites are missing.

Given the assumption of SGD to thermally stabilize thermal radiance variation at the sea surface over time, as shown for satellite images (Schubert et al., 2014; Oehler et al., 2017), we integrate several frames (thermal radiance images) to enhance the abovementioned focused SGD spots and to reveal further ones.

The thermal radiation variance of 10, 50 and 100 frames (integration of ~~~~2.5, 12.5 and 25 sec~~.~~ respectively) already indicates thermally stable (variance values <0.2) and thermally labile areas (variance values ≥0.2). However, with larger integration times of 300 and 670 frames (integration of ~~~~75 and 176 sec~~.~~ respectively), the three abovementioned focused SGD spots appear ~~plus~~, as well as two additional SGD spots in the upper part of the resulting variance image (lower right ~~image,~~panel in Fig. 3~~)~~), which spatially coincide with in-situ observed focused SGD sites 11/101, and 11/102. In the following sections, we focus on the three largely complete focused SGD spots 1 to 3 (Fig. 3). These three focused SGD spots exhibit variance values <0.019 and elliptical (~~1st~~first spot) to circular (~~2nd~~second and ~~3rd~~third spot) shapes at the sea~~-~~ surface underlined by the individual length/width ratios (Fig. 4). The lowest variance values, and therefore the thermally most stable areas ~~locate~~are located at the southern end of the ~~1st~~first and ~~2nd~~second SGD spot and on the northern end of the ~~3rd~~third SGD spot. Thermally indicated surface areas vary between 4.1 and 28.7~~-~~ m² ~~albeit the~~despite similar spring ~~depth~~depths of 13-20 m.

34.1 Spatiotemporal behaviour of discharge induced thermal radiance patterns

~~While the previous variance analysis highlights thermally stable and labile areas useful for identifying SGD spots it allows statements concerning the~~, time- specific information on spatiotemporal discharge behaviour ~~of each SGD spot only conditionally. These information will~~cannot be derived. We obtain this information through the introduction of transects (see left column ~~of Fig.~~in Figs. 5 and ~~Fig.6)~~6) along which we extract radiation values of each frame. The transects are constructed across the maximum spatial extent of each extracted, focused and diffuse SGD spot, as we expect ~~here~~ the most pristine temporal patterns representative for each spot to occur here.

34.1.1 Spatiotemporal behaviour of focused SGD spots

The middle column of Fig. 5 shows the time ~~sequences~~series of NTR values along each SGD transect. Furthermore, SGD spot boundaries are indicated (white lines =maximum gradients of each transect profile), which provide an orientation for the spatiotemporal behaviour of each spot. The focus is set on the area in between the boundaries representing the area in which SGD governs the thermal radiation distribution. In the case of the ~~1st~~first focused SGD spot that corresponds to sampled spring 11/103, the location is rather stable with its centre between transect pixel 18 and 23 (spatial shift of <0.~~65m~~65 m). In contrast, its boundaries are highly dynamic resulting in a varying distance between 20 and 31 ~~pixel (~~pixels (2.~~6m~~6 to 4.~~0m~~0 m respectively; for 90% of the data) and thus a change of ~~55~~155% (Table 1). This dynamic partially follows a certain trend during which both boundaries (white lines) show a synchronous directional change over a certain period (e.g. frame 150-400). Within the SGD spot, NTR values peak around the transect centre and decrease towards both boundaries. This peak is higher during the first 300 frames with NTR values ~~~~of 0.24 and decreases slightly between frames 300 to 500 to values of 0.08 before it increases to values around 0.18 for the remaining frames.

The centre of the ~~2nd~~second focused SGD spot, which corresponds to sampled spring 12/382, shifts between transect pixel 40 to 45 (<0.~~65m~~65 m), indicating similar stable conditions~~, while the~~. The boundary behaviour differs slightly ~~differs~~ from the ~~1st~~first focused SGD spot. The lower boundary is rather stable, fluctuating around transect pixel 70, whereas the upper boundary describes on average a wave-like change between frames 1 and 300 before displaying a stable fluctuation around transect pixel 20. The resulting diameter of the ~~2nd~~second focused SGD spot is therefore between 43 and 60 ~~pixel (~~pixels (5.59 to 7.~~8m~~8 m; for 90% of the data) and thus ~~show~~shows a change of ~~39~~139% (Table 1).

Compared to ~~1st~~the first focused SGD spot, the absolute peak values of the ~~2nd~~second focused SGD spot of -0.26 and their general trend over time are lower. They display a rather random behaviour over all frames with the exception of frames 485 to 520 during which the peak values (around -0.17) are higher.

The location of the ~~3rd~~third focused SGD spot, which corresponds to sampled spring 11/102, centres between transect pixel 15 to 20~~ is as stable as the latter.~~. The spot's boundaries are stable during the first 200 frames~~ during which~~, where they display a synchronous directional change similar to the ~~1st~~first focused SGD spot. For the remaining frames, the lower

boundary is highly dynamic and totally random while the upper is rather stable with less fluctuation until frame 350 ~~before it also starts to become highly dynamic with random change.~~. The resulting boundary distance ~~between~~within the first 200 frames is between 18 to 21 ~~pixel (~~pixels (2.~~34m~~34 to 2.~~73m~~73 m respectively; for 90% of the data) and thus ~~resemble~~resembles a change of ~~16~~116% (Table 1). The peak values of -0.08 to 0.06 resemble those of the ~~1st~~first and to a lesser extent those of the ~~2nd~~second focused SGD spot. Over time, they exhibit a similar random behaviour over all frames with the exception of frames 485 to 520 during which the peak values are higher ~~with values of ~~at 0.06.

3~~4~~.1.2 Spatiotemporal behaviour of diffuse SGD spots

~~Analogous to the focused SGD spots, the middle column of Fig~~. 6 shows time ~~sequences~~series of the NTR values along the transects of each diffuse SGD spot to illuminate the spatiotemporal discharge behaviour. Apparent for the ~~1st, 2nd~~first, second, and ~~3rd~~third diffuse SGD spots are higher NTR values > 4 for a constant transect length of 5-8 pixel ~~(~~(0.~~65m~~65-1.~~02m~~02 m) starting at the shoreline. Only the ~~4th~~fourth diffuse SGD spot exhibits no constantly elevated NTR values over the entire observation time close to the shoreline. All spots ~~have in common to~~ show outburst-like events during which NTR values > 3 occur. ~~Between~~Among all, the onsets and influence lengths of ~~these~~these outburst events vary. While for the first spot the average influence length reaches 20 ~~pixel~~pixels (=2.~~60m~~60 m) for NTR values >3, the average lengths of the second is 33 ~~pixel~~pixels (=4.~~29m), the~~29 m). The third has a length of 20 ~~pixel~~pixels (2.~~60m~~60 m) and the fourth only 7 ~~pixel~~pixels (0.~~91m). Consequentially~~91 m). Consequently, the percentage change of the influence length axis is between 150% for the first and third diffuse SGD spot, but amounts to 266% for the second spot, and reaches up to 600% for the fourth spot.

3

4.2 Periodicity analysis

The previous spatiotemporal behaviour already pointed at a certain recurrence pattern of the observed thermal radiation but lacked a distinct statement on whether or not it contains a significant periodicity and thus a dominating ~~forcing~~force inducing it. In order to provide ~~a clear~~an unequivocally and temporally ~~mostly~~ pristine discharge signal, we analyse its temporal pattern based on a single pixel of each transect (midpoint of the transect) using a temporal autocorrelation analysis (~~see~~ right column in ~~Fig~~Figs. 5 and ~~Fig.~~6 respectively).

3~~4~~.2.1 Periodicity of focused SGD spots

Temporal autocorrelation of the ~~1st~~first focused SGD spot distinctively differs from the ~~2nd~~second and ~~3rd~~third focused SGD spots. The ~~1st~~first spot shows a small but significant negative autocorrelation of -0.25 between lags (frames) 268 and 367 ~~(~~(64-92 ~~seconds~~sec) indicating a recurring pattern and hence a certain periodicity (Fig. 5). This observation matches the aforementioned peak value shift from 0.24 to 0.08 at the same frame region. The ~~2nd~~second focused SGD spot shows a small positive autocorrelation of 0.21 at lag (frame) 80, while remaining peaks vary in both directions, but below the confidence intervals. Both facts are distinctively different ~~to~~from the autocorrelation of the ~~1st~~first focused SGD spot, but

resemble the autocorrelation function of the ~~3rd~~third SGD spot, whose peaks are exclusively insignificant and ~~reflecting~~reflect no periodicity indication.

34.2.2 Periodicity of diffuse SGD spots

Time ~~sequence~~series plots (middle column in Fig. 6) ~~already~~ indicate a regular recurrence of thermal radiation values. This behaviour is underlined by the temporal autocorrelation of all diffuse SGD spots, which show a significant temporal autocorrelation that occurs at different lags and with mostly ~~with~~ different intensities ~~(Fig. 4).~~. While the ~~1st~~first diffuse SGD spot exhibits only one significant period at lag 81 ~~(~~(20 ~~seconds~~sec), the ~~2nd~~second spot shows two, one at lag 81 and a second one at lag 247 ~~(~~(62 ~~seconds~~sec). Despite the spatial proximity of ~~~5m~~ca. 5 m to the ~~ones before~~first two diffuse SGD spots, the ~~3rd~~third diffuse SGD spot shows a different temporal autocorrelation with one significant peak at lag 143 ~~(~~(36 ~~seconds). Similarly~~sec). Also different is the ~~4th~~fourth spot, which exhibits two peaks at lag 198 ~~(~~(50 ~~seconds~~sec) and lag 314 ~~(~~(78 ~~seconds~~sec). All plots in the right column contain a reference autocorrelation function of a pixel close ~~at~~to the source point at the shoreline (transect pixel three). This reference ~~clearly~~ shows ~~a~~ high-~~frequent~~frequency behaviour unlike the ~~ones~~temporal, diffuse SGD, induced thermal radiation behaviour described before (except for the last diffuse SGD spot).

34.3 Water chemistry and inverse geochemical modelling

The sampled focused on SGD and onshore springs ~~display~~discharge with a temperature between 21 ~~and~~to 31.5°C. Though the groundwater of both focused SGD and onshore springs originates from the ~~same~~ freshwater JGA ~~they~~, the springs discharge brackish water with salinities (TDS) ranging between 4.87 g/l and 26.0 g/l with the tendency to be on average less saline onshore (TDS=12.8 g/l) compared to the ~~focussed~~focused SGD (TDS=20.1 g/l). The inverse geochemical modelling results indicate halite, aragonite and gypsum to be the most important minerals in solution, though ion exchange on clay minerals plays a significant role. ~~However, although~~Although discharge locations are very close, the amount of dissolved halite (0-0.01 mol/kg H_2O), aragonite (0-0.004 mol/kg H_2O) and gypsum (0-0.02 mol/kg H_2O) vary significantly between the different springs (Table 2). Translated into cavitation rates, ~~the different branches of the groundwater system, which feed the individual springs, dissolve 59–1.552 cm3 of halite, aragonite and gypsum per cubic meter of through-flowing groundwater~~emerging groundwater dissolves and relocates about 59–1.552 cm^3 of halite, aragonite and gypsum per cubic metre from the passed branches of the groundwater flow net into the Dead Sea. Following the abovementioned approach, those springs with the lowest water/rock interactions, which consequently emerge from the most mature karst pipes, are springs 09/857, 10/30 11/121, which all have values <79.8 cm^3 of halite, aragonite and gypsum per cubic metre of water. In contrast, springs 09/855, 09/856 or 11/102 possess values >714 cm^3 of halite, aragonite and gypsum per cubic metre water which proves a higher water/rock interaction and thus intense dissolution activity that can only occur in less mature karst pipes (Table 2). Focused SGD spots reflect values of 696 and 749 cm^3 (first and third spot respectively) and thus a less mature karst system, while the second focused SGD spot has the lowest value of 414 cm^3 of halite, aragonite and gypsum per cubic meter water and thus emerges from a more mature karst system.

45. Discussion

The high spatial and temporal resolutions of the thermal radiation data ~~clearly~~ show a highly dynamic setting with various discharge locations, patterns, and forces. Analysing the spatiotemporal behaviour of each SGD spot independent of its type reveals striking details: i) it enhances focused SGD patterns otherwise being camouflaged by strong lateral flow dynamics and sheds light on crossflow influences, ii) the spatiotemporal behaviour shows a thermal SGD pattern size variation over time of up to ~~55~~155% for focused SGDs and 600% for diffuse SGDs due to different flow dynamics, and iii) it reveals a periodicity for diffuse SGD. We discuss these aspects in the following sections and outline possible driving forces or causes, and conclude with ~~general remarks to~~ potentials for and limitations of the presented approach ~~and~~ including possible transferability to other locations.

45.1 Enhancing focused SGD

Deriving ~~clear~~unequivocal SGD indications from single frames such as in Fig. 3 ~~might be non~~ is not trivial, especially in a highly dynamic system as the one presented. For the present case, we suggest the following causes to be relevant:

(i) lateral flow dynamics induced by diffuse discharge with higher temperatures (see point (ii)) govern the investigated area and superimpose thermal radiance signals from vertical flow of focused SGD as mentioned in Mallast et al. (2013a), and

(ii) entrainment of ambient water during the turbulent ascent (buoyant jet) of groundwater to the sea ~~-~~ surface (Jirka, 2004) leads to a consequential adaption of temperature and thus the emitted thermal radiance,

(iii) potential groundwater discharge fluctuation with possibly very small to stagnant discharge rates, as described in Ionescu et al. (2012) for the presented site~~,~~ at the moment of recording, which lead to no traceable thermal radiance signal from SGD at the sea surface.

However, the abovementioned possible relevant causes ~~have in common to be~~are all dynamic in spatial and temporal terms. Thus, accounting for the fact of a thermal stabilization at the sea surface as a consequence of a continuous discharge of equally tempered groundwater (Siebert et al., 2014) reveals thermally stable area induced by SGD that might otherwise be ~~not detectable.~~undetectable. The thermal stabilization is accompanied by the interplay of fluid movements (lateral vs. vertical flow kinetics) and thus ~~resulting and~~results in developing water surface geometries (wave structures~~)~~), e.g. at the interface of opposing water flows. Surface geometries have an effect on the recorded thermal radiances due to the directional dependence of the surface emissivity (Norman and Becker, 1995; Cheng and Liang, 2014). Wave fronts, for example, with surfaces being orthogonal to the sensor (0°~~)~~°), would have the highest thermal radiance values. As the angle to the sensor increases, recorded thermal radiances decrease, although the sea surface ~~-~~ temperature is the same (Cheng and Liang, 2014). Thus, the temporal effects through ~~a~~ thermal stabilization and changing surface geometries as a consequence of flow dynamics are the two governing drivers, which allow ~~to easily detecting~~easy detection of focused SGD through the integration of thermal radiation over longer time periods. According to our findings, the thermal radiance variance over a period of 25 ~~seconds~~sec

(100 frames) already provides a sufficient basis to outline SGD areas (Fig. 2). Integrating over longer time periods ~~even~~ emphasizes SGD areas, which consequently confirms the thermal radiance stabilization over time at the sea surface of a SGD-affected area (Siebert et al., 2014).

Apart from enhancing focused SGD occurrences, the shape of the focused SGD variance pattern at the sea surface along with the location of the lowest variance values (area most thermally ~~most~~ stable~~ area~~) gives an indication of SGD emergence locations and the deflection of the resulting vertical plume until it reaches the sea surface. None of the three are perfectly circular which would refer to an uninfluenced positive buoyancy of discharging water and a SGD emergence directly beneath the centre of the variance pattern (Jirka, 2004). Instead, they all are more or less ~~elliptic~~elliptical with lowest variance values at the southern ~~(1st~~ends (first and ~~2nd~~second focused SGD spot) and at the northern ends (~~3rd~~third focused SGD spot). The remarkable ~~elliptic~~elliptical shape of the ~~1st~~first focussed SGD spot implies a crossflow from the south causing a northward deflection of the vertical SGD plume and an elliptic shape of the horizontal plume pattern at the sea surface (Akar and Jirka, 1995). ~~The~~ Less pronounced elliptical shapes but with the same northward deflection ~~with less pronounced elliptic shapes~~ trend exhibit the ~~2nd~~second and ~~3rd~~third focused SGD spot. ~~This~~The northward deflection is most likely induced by flow dynamics as a consequence of diffuse SGD. Since the location of the diffuse SGD spots, especially those with distinctively periodic events with higher discharge rates (Fig. ~~4~~3), is directly SSW and shows the same northward horizontal plume orientation, we suggest this discharge ~~to be~~is the driving force for the deflection.

4~~5~~.2 Spatiotemporal behaviour of SGD patterns

The variance image provides an average representation of all SGD spots, which are especially useful for reliable size/discharge comparison purposes between SGD spots and likewise allow outlining SGD spots. However, as the previous section ~~already~~ points out, all are subject to external forces such as currents, waves~~ but also~~, and the influence of internal discharge dynamics ~~influencing~~on resulting pattern shape and size characteristics of the thermal radiance pattern over time.

For focused SGD, the observed thermal radiance pattern sizes (distance between boundaries) over time show a spatial variation between ~~16~~116% (=2.~~3m~~3 m for the first focused SGD spot) and ~~55~~155% (=4.~~0m~~0 m for the third focused SGD spot~~).~~) as shown in Fig. 5. The variance is~~ clearly~~ a result of occurring lateral flow dynamics constantly influencing the pattern on the sea surface. Yet, the influence is anisotropic in space and time as the lateral flow dynamics are dominated by waves coming from the ~~East~~east, the interaction of horizontal SGD plumes on the sea surface (e.g. ~~2nd~~second and ~~3rd~~third focused SGD) as described in Teamah and Khairat (2015), but moreover the strong lateral flow dynamics (crossflow) induced by the discharge impulses of diffuse SGD that in the following is deflected to the NE. The interplay and constant temporal changes lead to an asynchronous boundary movement for most of the observed SGD induced thermal radiance patterns that it is only partly changing to a synchronous movement as for the ~~1st~~first and ~~3rd~~third focused SGD spot during the first 200 frames. During this time only one force seems to dominate the dynamic, causing the synchronous behaviour.

The SGD induced thermal radiation pattern size variation is different for the observed diffuse SGD spots. While three out of four spots constantly influence ~~an~~a longshore area of 5-8 ~~pixel (~~pixels (0.65-1.~~04m) along the shoreline,~~04 m), outburst-like

events change the cross-shore influence length ~~perpendicular to the shoreline~~ between 150-600 % and ~~between ~~0.60-4.~~29m.~~29 m (Fig. 6). The constant influence reflects a continuous diffuse discharge with lower discharge rates. The latter however ~~clearly~~ shows a focused flow with intermittent higher discharge rates. Higher discharge rates induce a higher momentum and consequentially ~~increases~~increase the influenced area off the discharge spot. In turn it reveals that karst conduits ~~to~~ exist ~~already~~ close to the shoreline and next to diffuse SGD. The intermittency with a seemingly ~~reccurring~~recurring temporal pattern, however, points ~~at~~to a steady interplay of different forces that is the subject ~~to~~of the next section.

45.3 Periodicity of diffuse SGD

For focused SGD spots, we could not reveal a significant periodicity, either because of the limited observation length or because no periodicity exists. For diffuse SGD spots, the temporal autocorrelation analysis reveals significant periodicities. The periodicity of discharge rate events varies significantly among given spots between 20 to 78 ~~seconds~~sec (right column ~~of~~in Fig. ~~4). Primarily, it~~6). It primarily provides a further example of the high temporal discharge variability ~~even~~ over small spatial scales which, normally, is due to tides or wave-setup that change hydrostatic pressure conditions (Taniguchi et al., 2003b; Burnett et al., 2006). For the present case, tidal influences are irrelevant as the tidal cycles do not exist at the study site. Wave influence on the other hand cannot be excluded, per se. However, most likely it is not the main cause since observed wave frequency of 3~~-7 seconds~~ to7 sec would cause high-frequency discharge intermittency of the same magnitude. Precisely this high frequency is observable in the autocorrelation graphs of Fig. ~~4~~6 close to the shoreline (transect pixel 3). ~~Yet, it likewise~~Thus, the frequency proves the minor wave influence on the main discharge events with an observed frequency that is up to 10 magnitudes larger. Along with the focused discharge nature, it rather points ~~at~~to an interplay ~~of~~between wave-setup and a geometry effect within conduits of groundwater flow as the underlying mechanism as described for karst areas in Smart and Ford (1986). Discharge behaviour in this case depends on the maturity and geometric formation of the conduit network, is therefore highly anisotropic~~,~~ and heterogeneous, and features a rapid flow (Surić et al., 2015). ~~Especially anisotropy and heterogeneity can likewise be observed for~~The anisotropic and heterogeneous discharge behaviour is furthermore underlined by the discharge ~~behaviour of all SGD spots since neither discharge~~ onset ~~nor~~and the periodicity ~~agrees~~that is unequal among the individual spots, even though their spatial location is within ~~10m~~10 m distance~~.~~ (Fig. 3). Plus, According to the modelling results, groundwater passes the DSG through ~~the existence of~~ several subaquifers as described in Yechieli et al. (2010~~)~~), and most probably via conduits ~~can~~, which develop through the fuzzy dissolution of easily soluble minerals ~~aragonite, gypsum, and halite contained in~~ that make up large percentages of the sedimentary body. It is further assumed, due to the impregnation of the sediment~~. These conduits are assumed to be less mature close to the shoreline, as~~ by Dead Sea brine, that cavitation activity is lower closer and below the fresh~~-~~/saltwater interface ~~is moving lake wards with dropping lake level and the subsequently dropping groundwater tables. Thus, in these areas the time of freshwater being in contact with dissolvable~~ , although it exists and leads to abundant submarine springs. However, groundwater may also reach the Dead Sea through open faults, which may deeply fracture the sedimentary body as a result

of active rift tectonics. Further preferential groundwater pathways may also be created through shallow cracks that develop through the relaxation of the sediment ~~is short which leads to~~ due to the gravitational release of interstitial brine.

~~However,~~ for whatever reason fresh groundwater is allowed to invade the DSG due to the omnipresent abundance of easily soluble minerals, dissolution activities will immediately start and will enlarge hydraulic apertures of the initial ~~karstification status. However, due to the fuzziness of the process, even in this initial karstification area, the cavitation~~ pathways through the sedimentary body. Cavitation rates ~~vary~~may be dependent on boundary conditions (e.g. supply of fresh water, hydraulic gradient and microbial activity) leading to different degrees of conduit maturity~~. Consequentially~~ and random conduit/network geometry.

~~Consequently~~, it is thoroughly possible that an initial anisotropic ~~karst system exists onshore and especially around the shoreline. This system is certainly less developed as the one described for focused SGD spots in Ionescu et al. (2012) yet similar anisotropic.~~flow system is about to develop close to the observed shoreline. In interaction with the wave setup, we suggest ~~the~~that such a randomly developed initial ~~karst~~flow system ~~to be~~is the cause for the different onsets and influence areas for the observed outburst-like events.

~~**4.3 General remarks**~~

5. 4 Potentials, limitations and potential errors

The hovering of the UAV over a predefined location and the sensing of thermal radiation at a rate of 4-~~5Hz~~5 Hz allows ~~combining~~a combination of the continuous ~~spatial~~temporal with the continuous spatial scale~~. Thus~~ for SGD research. In this context it bears an enormous potential as it is possible to provide detailed and high resolution information on SGD dynamics but also on external forces influencing it. ~~Despite the short total observation time of the present study it shows a temporal discharge behaviour in the range of 101-102 seconds. Classical in-situ measurements however usually have measuring~~The potential includes the high temporal resolution (sampling intervals) which differs by the order of one magnitude to classical in-situ measurement intervals of 10^1-10^2 minutes (Cable et al., 1997; Mulligan and Charette, 2006; Michael et al., 2011~~) and thus differ by~~), allowing the ~~order~~illumination of ~~one magnitude. These intervals could not reflect the observed~~ short-term discharge dynamics~~. Moreover,~~ that could not be reflected with classical methods. The potential furthermore concerns the spatiotemporal continuous ~~results also provide~~characteristic of the presented approach. With the unequivocal indication ~~on suitable and unsuitable sampling sites in spatial terms. E.g. with the clear indication on~~regarding where diffuse or focused SGD occurs, and where exactly the transition between ~~diffuse~~ SGD ~~with a focused SGD nature~~and ambient fluids is, ~~indicates~~the indication is that proper sampling sites for each of them~~, that~~ could not ~~be~~have been done with a subjective selection of sampling sites. Thus, applying the presented approach before pursuing in-situ sampling (which includes the selection of proper sampling sites and sampling intervals) is undoubtedly advantageous.

It is likewise advantageous forThe third potential concerns SGD monitoring and especially SGD quantification purposes. Recalling from the introduction, the basis for SGD quantification is the size of thermal radiance patterns (plumes) in most

studies (Kelly et al., 2013; Mallast et al., 2013a; Tamborski et al., 2015; Lee et al., 2016). The presented results show a spatial variation of 150-600% ~~for diffuse SGD~~ which indicates the possible uncertainty that underlies a quantification based on single thermal infrared images. With the presented approach these uncertainties could be specified, which, in turn, increases the explanatory power of the quantification.

In this context

Apart from these potentials, the ~~question arises on the transferability of~~ approach bears limitations and potential errors that need to be accounted for, if the presented approach~~. In general~~ is to transfer to different locations. The first limitation concerns the need for rigid image parts, such as land, to be able to pursue a proper image registration. Equal share of land and water parts, as in the present case, increases the accuracy and thus reduces the potential error due to an erroneous intensity-based image registration, but reduces the investigable area spatially and limits it to areas close to the shoreline. The shoreline-bond could be overcome by using rigidly fixed buoys and mounted aluminium plates on top as ground control points anchored offshore. While the investigable area is maximized, the image registration needs to be changed to a procedure based on control points to determine the image transformation and thus the registration as described, for example, in Holman et al. (2017), since the intensity of an image cannot be taken as the basis.

However, independent of the selected approach and the land/water share, flight altitude and camera lens define the size of the footprint and thus the spatial coverage. Due to regulatory framework, flight altitudes are usually restricted which consequently limits the maximum possible footprint. Thus the restricted flight altitudes represent another spatial limitation of the approach.

The aforementioned spatial limitations are furthermore accompanied by temporal limitations and errors. These temporal limitations are given by the flight times of present-day UAVs that reach up to tens of minutes (Floreano and Wood, 2015). Continuous investigations for several hours, days, or beyond are, to date, impossible. This sort of long-term and continuous investigation for monitoring purposes, for example, could be possible using a thermal camera system fixed to a mast making flight times irrelevant. Despite other factors coming into play with fixed cameras, such as the viewing angle dependency on emissivity (Norman and Becker, 1995) and the addition of a changing solar reflection component to thermal emission during the day vs. solely thermal emission during the night, the potential lies in the generation of a thermal radiation time series and trend analyses, for example. Similar approaches using fixed video and camera systems, operating in the visible spectrum (RGB), are operational for near-shore monitoring and management purposes (Holman et al., 2003; Taborda and Silva, 2012). Adapting these operational approaches to fixed thermal camera systems would mean overcoming temporal limitations on the presented UAV approach and generating unforeseen potential in SGD research.

Further limitations are sensor-concerned. A geometric error can be introduced by lens characteristics which distort the thermal image. Especially a wide-angle lens produces geometric distortions (Meier et al., 2011; Vidas et al., 2012) that can be corrected in order to achieve an image projection that matches the true projection surface. A further sensor limitation is a possible radiometric error. All uncooled microbolometers, as the one applied, have the disadvantage that a thermal drift could occur (Mesas-Carrascosa et al., 2018). Caused by effects of the ambient temperature on the microbolometer detector

housing and the consequential energy dissipation from the housing onto the detector array, the thermal drift leads to a non-uniform influence on the thermal image, which manifests in a vignetting effect with radiance reduction towards the borders of a recorded image relative to its projection centre (Meier et al., 2011). Since it additionally changes with time (Wolf et al., 2016), this drift, especially for long term investigations, needs to be accounted for, otherwise Mesas-Carrascosa et al. (2018) estimate the temperature error to increase by 0.7°C per minute.

The aforementioned limitations are all of technical nature. However, we need to emphasize that natural limitations may also exist that may affect the result. The most prominent factor is the temperature difference between groundwater and ambient water. With a difference approaching 0°C, an unequivocal differentiation is almost impossible, especially if we include entrainment of ambient water and thus the temperature adaption. The higher the difference is, the more likely is the possibility of identifying SGD induced thermal anomalies in single images, but also of using a time-series of thermal radiance images – as in the presented approach. The advantage of time-series data is that the temporal dimension includes dynamics which may enhance subtle temperature differences. These dynamics may be due to waves in which the surface geometries provide the direct indication rather than the surface temperature (recall the directional dependence of the surface emissivity on recorded radiances - see section 5.1). Hence, time series data, whether from an UAV platform or from a mast is thoroughly recommendable.

Further limitations may exist due to parallel existing strong lateral flow dynamics as in the present case. On single thermal radiation images, these dynamics may camouflage further focused SGD sites, especially at sites with low groundwater-ambient water temperature differences. Strong lateral dynamics may also, as in the present case, camouflage any bathymetry effect on thermal radiation images as it is described in Xie et al. (2002). If bathymetry has affected the sea surface temperature, we could detect a gradual decrease in temperature from the shoreline towards the sea centre. The reason that we cannot detect any gradual decrease, apart from the camouflaging lateral flow dynamics, may be the bathymetry itself. While the bathymetry decreases gradually during the first 30 m until about 10 m, SGD is found at the bottom of steep walls in depths of up to 30 m (Ionescu et al., 2012) in distances of 50 m to the coastline, which is also visible in Fig. 1a. This sudden morphological step may additionally cause the disappearance of the gradual temperature decrease usually triggered by bathymetry. However, we cannot exclude this effect occurring in other places and different settings where, for example, the bathymetry consists of uniform slopes <5°. In these occasions, the bathymetry would cause higher sea surface temperatures in summer and lower sea surface temperatures in winter that may be accounted for in the case of SGD detection.

As pointed out, for most technical limitations, solutions and corrections exit to improve and adopt the presented approach independent of the study sites' characteristics. Thus, we propose that the approach ~~to be~~is applicable to other areas with diffuse or focused SGD, since the ~~method requires~~general requirements consist of an UAV with a mounted thermal camera system ~~only~~ and ~~some~~ rigid areas or fixed points~~/area~~ within the covered footprint to allow a proper co-registration of all ~~frames. Recommendable is furthermore a temperature difference of groundwater and ambient water allowing a clear~~

~~differentiation~~thermal images. The applicability of the presented approach concerning natural limitations needs to be investigated in the future. However, given a certain discharge rate and sufficient temperature differences between groundwater and ambient water, the suggestion is that time series data of thermal radiance images could prove to be a promising tool for SGD investigations.

5

6. Conclusion

Hovering with ~~a~~an UAV over a predefined location recording thermal radiances at a temporal resolution of 4-~~5Hz~~5 Hz is a novel application technique combining continuous spatial and temporal scales. Based on the combination, we enhance focused SGD patterns that are otherwise ~~being~~ camouflaged by strong lateral flow dynamics that may not be observed on single thermal radiation images. We furthermore show the spatiotemporal behaviour of a SGD induced thermal radiation pattern to vary in size and over time by up to ~~55~~155% for focused SGDs and by up to 600% for diffuse SGDs due to different underlying flow dynamics. We want to ~~emphasize~~emphasise this aspect as it is important for SGD monitoring and especially SGD quantification purposes, which rely on single thermal radiation images and thus temporal snapshots ~~which~~that may not provide the entire picture. And lastly, we are able to reveal a short-term periodicity in the order of 20 to 78 ~~seconds~~sec for diffuse SGD, which we attribute to an interplay ~~of~~between conduit maturity/geometry and wave setup. The observed periodicity differs ~~by~~in the order of a magnitude to classical in-situ measurement intervals, which would not be able to detect the temporal behaviour we observe.

Since SGD, independent of its type, is highly heterogeneous in space and time, as we have also shown in our study, we suggest, where possible, ~~to include~~inclusion of the presented approach before any in-situ sampling to identify proper sampling locations and intervals. In ~~that~~this way, SGD investigations, especially in systems with complex flow, will be able to optimize their sampling strategies and ~~will~~ possibly improve their results.

Acknowledgements: This work was financed by the DESERVE Virtual Institute, funded by the Helmholtz Association of German Research Centers (VH-VI-527) and a scholarship from the German Federal Ministry of Education and Research (YSEP97). Personal thanks are addressed to Yossi Yechieli and Gideon Baer (both Geological Survey of Israel) for the kind support, ~~the~~ warm welcome, and unconditional assistance before and during the exchange of UM, including the logistical help. Meteorological Data were provided by KIT (Jutta Metzger). This manuscript has benefited from the efforts, insightful comments and additions of two anonymous reviewers to whom we are eternally grateful.

References

Akar, P. J., and Jirka, G. H.: Buoyant spreading processes in pollutant transport and mixing part 2: Upstream spreading in weak ambient current, Journal of Hydraulic Research, 33, 87-100, 1995.

Burg, A., Yechieli, Y., and Galili, U.: Response of a coastal hydrogeological system to a rapid decline in sea level; the case of Zuqim springs – The largest discharge area along the Dead Sea coast, Journal of Hydrology, 536, 222-235, https://doi.org/10.1016/j.jhydrol.2016.02.039, 2016.

Burnett, W. C., Aggarwal, P. K., Aureli, A., Bokuniewicz, H., Cable, J. E., Charette, M. A., Kontar, E., Krupa, S., Kulkarni, K. M., Loveless, A., Moore, W. S., Oberdorfer, J. A., Oliveira, J., Ozyurt, N., Povinec, P., Privitera, A. M. G., Rajar, R., Ramessur, R. T., Scholten, J., Stieglitz, T., Taniguchi, M., and Turner, J. V.: Quantifying submarine groundwater discharge in the coastal zone via multiple methods, Science of The Total Environment, 367, 498-543, 10.1016/j.scitotenv.2006.05.009, 2006.

Cable, J., Burnett, W., Chanton, J., Corbett, D., and Cable, P.: Field evaluation of seepage meters in the coastal marine environment, Estuarine, Coastal and Shelf Science, 45, 367-375, 1997.

Cheng, J., and Liang, S.: Effects of Thermal-Infrared Emissivity Directionality on Surface Broadband Emissivity and Longwave Net Radiation Estimation, IEEE Geoscience and Remote Sensing Letters, 11, 499-503, 10.1109/LGRS.2013.2270293, 2014.

Cortelezzi, L., and Karagozian, A. R.: On the formation of the counter-rotating vortex pair in transverse jets, Journal of Fluid Mechanics, 446, 347-373, 2001.

Floreano, D., and Wood, R. J.: Science, technology and the future of small autonomous drones, Nature, 521, 460, 10.1038/nature14542, 2015.

Holman, R., Stanley, J., and Ozkan-Haller, T.: Applying video sensor networks to nearshore environment monitoring, IEEE Pervasive Computing, 2, 14-21, 2003.

FLIR® Systems: Tau® 2 Uncooled Cores: http://www.flir.com/cores/display/?id=54717, access: 16.12.2016, 2016.

Ionescu, D., Siebert, C., Polerecky, L., Munwes, Y. Y., Lott, C., Häusler, S., Bižić-Ionescu, M., Quast, C., Peplies, J., Glöckner, F. O., Ramette, A., Rödiger, T., Dittmar, T., Oren, A., Geyer, S., Stärk, H.-J., Sauter, M., Licha, T., Laronne, J. B., and de Beer, D.: Microbial and Chemical Characterization of Underwater Fresh Water Springs in the Dead Sea, PLoS ONE, 7, e38319, 10.1371/journal.pone.0038319, 2012.

Holman, R. A., Holland, K. T., Lalejini, D. M., and Spansel, S. D.: Surf zone characterization from Unmanned Aerial Vehicle imagery, Ocean Dynamics, 61, 1927-1935, 10.1007/s10236-011-0447-y, 2011.

Holman, R. A., Brodie, K. L., and Spore, N. J.: Surf Zone Characterization Using a Small Quadcopter: Technical Issues and Procedures, IEEE Transactions on Geoscience and Remote Sensing, 55, 2017-2027, 10.1109/TGRS.2016.2635120, 2017.

Jirka, G. H.: Integral model for turbulent buoyant jets in unbounded stratified flows. Part I: Single round jet, Environmental Fluid Mechanics, 4, 1-56, 2004.

Johnson, A. G., Glenn, C. R., Burnett, W. C., Peterson, R. N., and Lucey, P. G.: Aerial infrared imaging reveals large nutrient-rich groundwater inputs to the ocean, Geophysical Research Letters, 35, L15606 15601-15606, 10.1029/2008gl034574, 2008.

Kelly, J. L., Glenn, C. R., and Lucey, P. G.: High-resolution aerial infrared mapping of groundwater discharge to the coastal ocean, Limnology and Oceanography: Methods, 11, 262-277, 10.4319/lom.2013.11.262, 2013.

Kim, J., and Fessler, J. A.: Intensity-based image registration using robust correlation coefficients, IEEE transactions on medical imaging, 23, 1430-1444, 2004.

Lee, E., Yoon, H., Hyun, S. P., Burnett, W. C., Koh, D. C., Ha, K., Kim, D. j., Kim, Y., and Kang, K. m.: Unmanned aerial vehicles (UAVs)-based thermal infrared (TIR) mapping, a novel approach to assess groundwater discharge into the coastal zone, Limnology and Oceanography: Methods, 14, 725-735, 10.1002/lom3.10132, 2016.

Lewandowski, J., Meinikmann, K., Ruhtz, T., Pöschke, F., and Kirillin, G.: Localization of lacustrine groundwater discharge (LGD) by airborne measurement of thermal infrared radiation, Remote Sensing of Environment, 138, 119-125, 2013.

Magal, E., Weisbrod, N., Yakirevich, A., Kurtzman, D., and Yechieli, Y.: Line-Source Multi-Tracer Test for Assessing High Groundwater Velocity, Ground Water, 48, 892-897, 10.1111/j.1745-6584.2010.00707.x, 2010.

Mallast, U., Schwonke, F., Gloaguen, R., Geyer, S., Sauter, M., and Siebert, C.: Airborne Thermal Data Identifies Groundwater Discharge at the North-Western Coast of the Dead Sea, Remote Sensing, 5, 6361, 2013a.

Mallast, U., Siebert, C., Wagner, B., Sauter, M., Gloaguen, R., Geyer, S., and Merz, R.: Localisation and temporal variability of groundwater discharge into the Dead Sea using thermal satellite data, Environmental Earth Sciences, 1-17, 10.1007/s12665-013-2371-6, 2013b.

Mallast, U., Gloaguen, R., Friesen, J., Rödiger, T., Geyer, S., Merz, R., and Siebert, C.: How to identify groundwater-caused thermal anomalies in lakes based on multi-temporal satellite data in semi-arid regions, Hydrol. Earth Syst. Sci., 18, 2773-2787, 10.5194/hess-18-2773-2014, 2014.

Meier, F., Scherer, D., Richters, J., and Christen, A.: Atmospheric correction of thermal-infrared imagery of the 3-D urban environment acquired in oblique viewing geometry, Atmos. Meas. Tech., 4, 909-922, 10.5194/amt-4-909-2011, 2011.

Mejías, M., Ballesteros, B. J., Antón-Pacheco, C., Domínguez, J. A., Garcia-Orellana, J., Garcia-Solsona, E., and Masqué, P.: Methodological study of submarine groundwater discharge from a karstic aquifer in the Western Mediterranean Sea, Journal of Hydrology, 464–465, 27-40, 10.1016/j.jhydrol.2012.06.020, 2012.

Mesas-Carrascosa, F.-J., Pérez-Porras, F., Meroño de Larriva, J., Mena Frau, C., Agüera-Vega, F., Carvajal-Ramírez, F., Martínez-Carricondo, P., and García-Ferrer, A.: Drift Correction of Lightweight Microbolometer Thermal Sensors On-Board Unmanned Aerial Vehicles, Remote Sensing, 10, 615, 2018.

Michael, H. A., Lubetsky, J. S., and Harvey, C. F.: Characterizing submarine groundwater discharge: a seepage meter study in Waquoit Bay, Massachusetts, Geophysical Research Letters, 30, 2003.

Michael, H. A., Charette, M. A., and Harvey, C. F.: Patterns and variability of groundwater flow and radium activity at the coast: A case study from Waquoit Bay, Massachusetts, Marine Chemistry, 127, 100-114, http://dx.doi.org/10.1016/j.marchem.2011.08.001, 2011.

Mulligan, A. E., and Charette, M. A.: Intercomparison of submarine groundwater discharge estimates from a sandy unconfined aquifer, Journal of Hydrology, 327, 411-425, 2006.

Norman, J. M., and Becker, F.: Terminology in thermal infrared remote sensing of natural surfaces, Remote Sensing Reviews, 12, 159-173, 10.1080/02757259509532284, 1995.

Oehler, T., Eiche, E., Putra, D., Adyasari, D., Hennig, H., Mallast, U., and Moosdorf, N.: Timing of land-ocean groundwater nutrient fluxes from a tropical karstic region (southern Java, Indonesia), Hydrol. Earth Syst. Sci. Discuss., 2017, 1-18, 10.5194/hess-2017-621, 2017.

Schubert, M., Scholten, J., Schmidt, A., Comanducci, J. F., Pham, M. K., Mallast, U., and Knoeller, K.: Submarine Groundwater Discharge at a Single Spot Location: Evaluation of Different Detection Approaches, Water, 6, 584-601, 2014.

Siebert, C., Rödiger, T., Mallast, U., Gräbe, A., Guttman, J., Laronne, J. B., Storz-Peretz, Y., Greenman, A., Salameh, E., and Al-Raggad, M.: Challenges to estimate surface-and groundwater flow in arid regions: The Dead Sea catchment, Science of the Total Environment, 485, 828-841, 2014.

Smart, C., and Ford, D.: Structure and function of a conduit aquifer, Canadian Journal of Earth Sciences, 23, 919-929, 1986.

Surić, M., Lončarić, R., Buzjak, N., Schultz, S. T., Šangulin, J., Maldini, K., and Tomas, D.: Influence of submarine groundwater discharge on seawater properties in Rovanjska-Modrič karst region (Croatia), Environmental Earth Sciences, 74, 5625-5638, 10.1007/s12665-015-4577-2, 2015.

Swarzenski, P. W., Reich, C. D., Spechler, R. M., Kindinger, J. L., and Moore, W. S.: Using multiple geochemical tracers to characterize the hydrogeology of the submarine spring off Crescent Beach, Florida, Chemical Geology, 179, 187-202, https://doi.org/10.1016/S0009-2541(01)00322-9, 2001.

Taborda, R., and Silva, A.: COSMOS: A lightweight coastal video monitoring system, Computers & geosciences, 49, 248-255, 2012.

Tamborski, J. J., Rogers, A. D., Bokuniewicz, H. J., Cochran, J. K., and Young, C. R.: Identification and quantification of diffuse fresh submarine groundwater discharge via airborne thermal infrared remote sensing, Remote Sensing of Environment, 171, 202-217, http://dx.doi.org/10.1016/j.rse.2015.10.010, 2015.

Taniguchi, M., Burnett, W. C., Cable, J. E., and Turner, J. V.: Assessment methodologies for submarine groundwater discharge, in: Land and Marine Hydrogeology, edited by: Taniguchi, M., Wang, K., and Gamo, T., Elsevier, Amsterdam, 1-23, 2003a.

Taniguchi, M., Burnett, W. C., Smith, C. F., Paulsen, R. J., O'Rourke, D., Krupa, S. L., and Christoff, J. L.: Spatial and temporal distributions of submarine groundwater discharge rates obtained from various types of seepage meters at a site in the Northeastern Gulf of Mexico, Biogeochemistry, 66, 35-53, 10.1023/B:BIOG.0000006090.25949.8d, 2003b.

TeAx Technology: Thermal Capture http://thermalcapture.com/category/products/recordingsolutions/, access: 16.12.2016, 2016.

Tzanetakis, G., and Cook, P.: Musical genre classification of audio signals, IEEE Transactions on speech and audio processing, 10, 293-302, 2002.

Vollmer, M.: Newton's law of cooling revisited, European Journal of Physics, 30, 1063, 2009.

Viana, I., Orteu, J.-J., Cornille, N., and Bugarin, F.: Inspection of aeronautical mechanical parts with a pan-tilt-zoom camera: an approach guided by the computer-aided design model, Journal of Electronic Imaging, 24, 061118, 2015.

Vidas, S., Lakemond, R., Denman, S., Fookes, C., Sridharan, S., and Wark, T.: A mask-based approach for the geometric calibration of thermal-infrared cameras, IEEE Transactions on Instrumentation and Measurement, 61, 1625-1635, 2012.

Wolf, A., Pezoa, J. E., and Figueroa, M.: Modeling and Compensating Temperature-Dependent Non-Uniformity Noise in IR Microbolometer Cameras, Sensors (Basel, Switzerland), 16, 1121, 10.3390/s16071121, 2016.

Xie, S.-P., Hafner, J., Tanimoto, Y., Liu, W. T., Tokinaga, H., and Xu, H.: Bathymetric effect on the winter sea surface temperature and climate of the Yellow and East China Seas, Geophysical Research Letters, 29, 81-81-81-84, doi:10.1029/2002GL015884, 2002.

Yechieli, Y., Ronen, D., Berkowitz, B., Dershowitz, W. S., and Hadad, A.: Aquifer Characteristics Derived From the Interaction Between Water Levels of a Terminal Lake (Dead Sea) and an Adjacent Aquifer, Water Resources Research, 31, 893-902, 10.1029/94wr03154, 1995.

Yechieli, Y., Shalev, E., Wollman, S., Kiro, Y., and Kafri, U.: Response of the Mediterranean and Dead Sea coastal aquifers to sea level variations, Water Resoures Research, 46, W12550 12551-12511, 10.1029/2009wr008708, 2010.

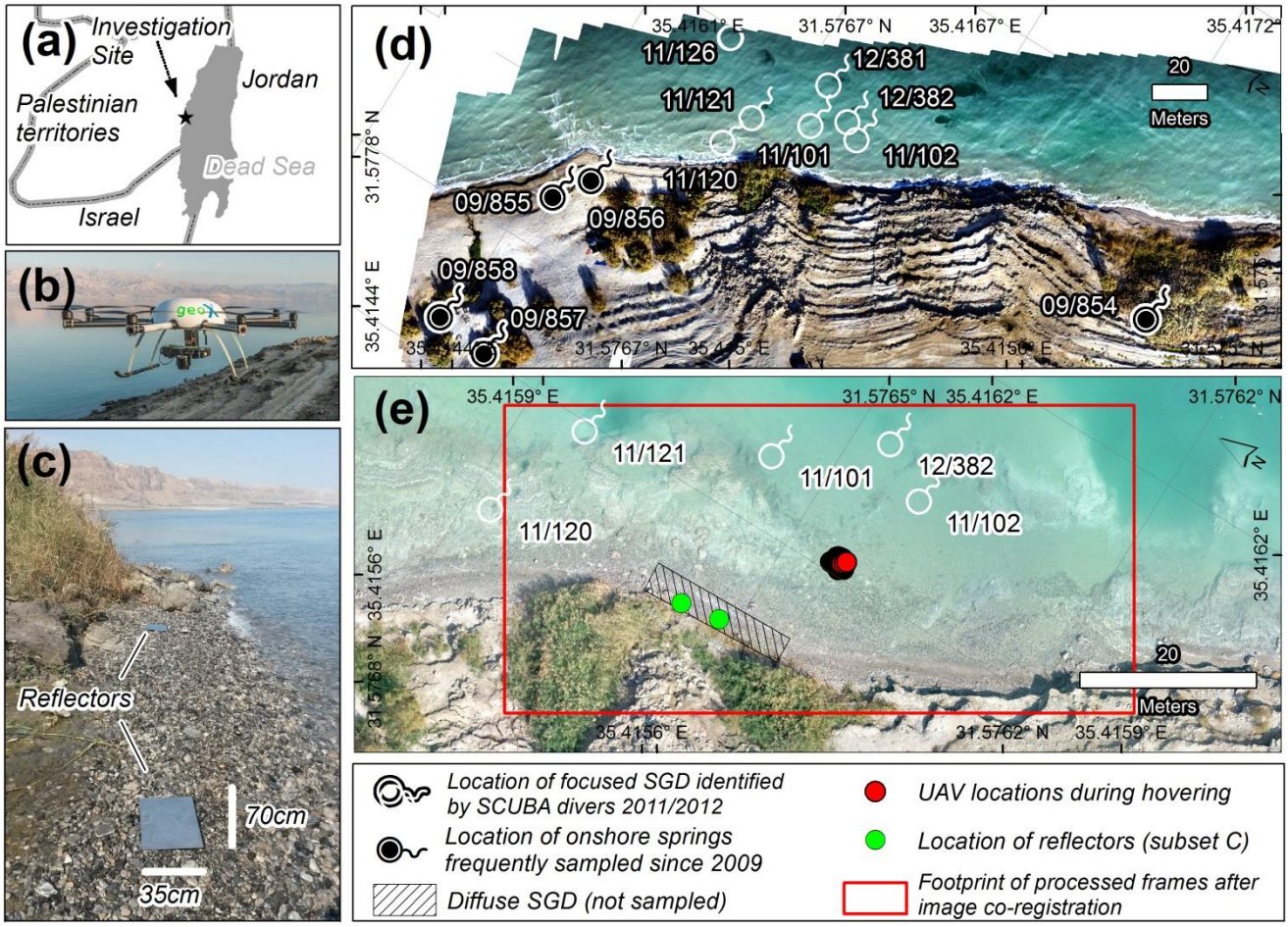

Figure 1: Location of the study area in at the Dead Sea (A), photo of the UAV used during the study (B), photo of both reflectors at the covered coastline section (C), distribution of focused SGD spots identified and sampled by divers in the years 2011 and 2012, and onshore springs which have been sampled frequently since 2009 (D), and aerial photograph from 10 February ~~10th,~~ 2016 at 12:~~11 p.m.~~11pm local time of the covered area along with UAV positions during hovering, location of reflectors, the footprint of the processed frames after co-registration described in section 2.3 and locations of observe diffuse SGD (E).

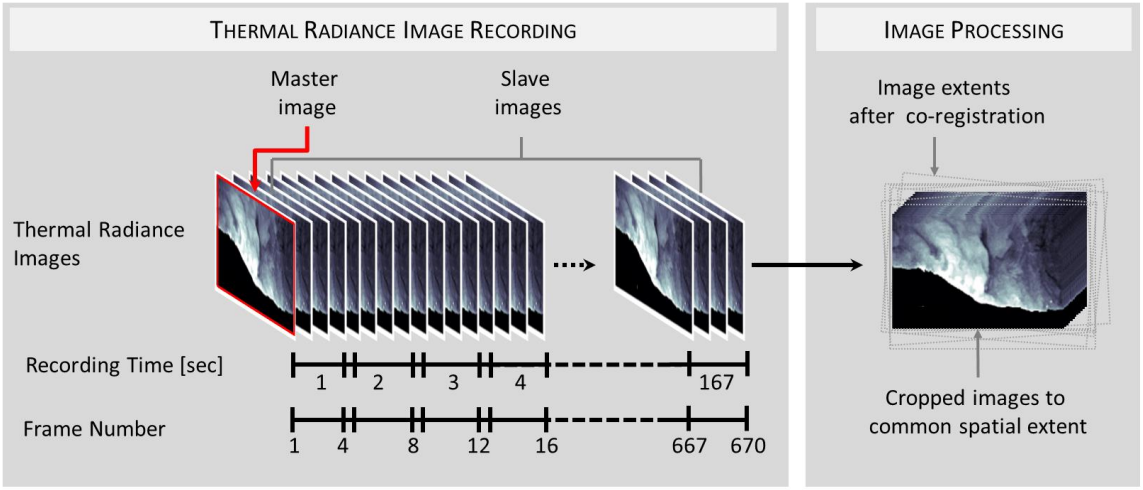

Figure 2: ~~Graphical~~Graphic illustration of image recording and image pre-processing applied during the presented approach.

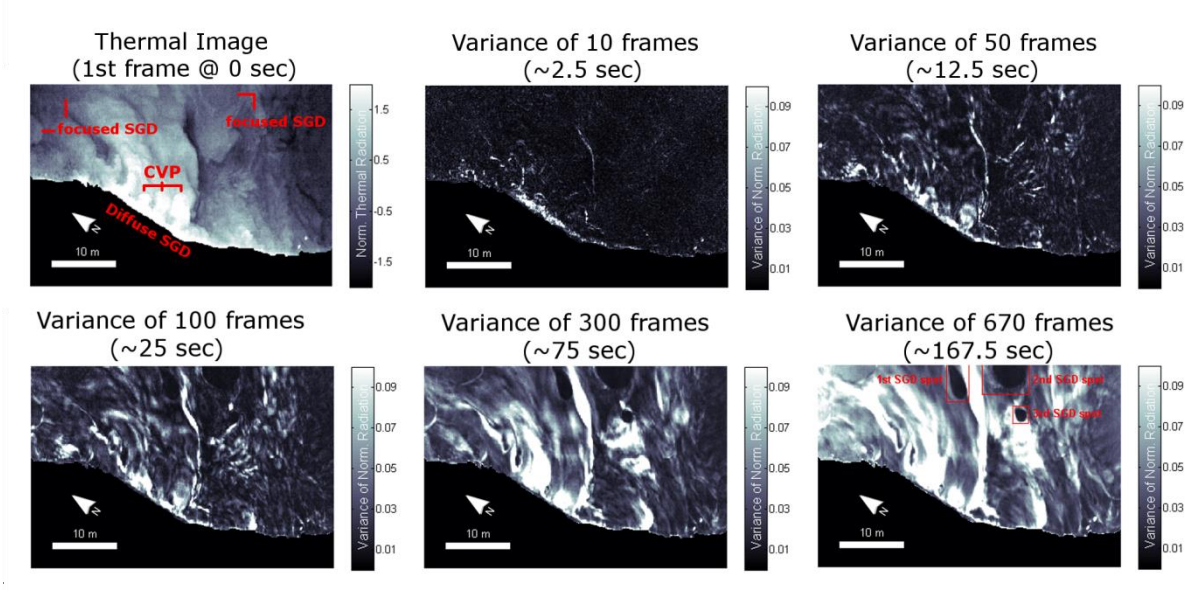

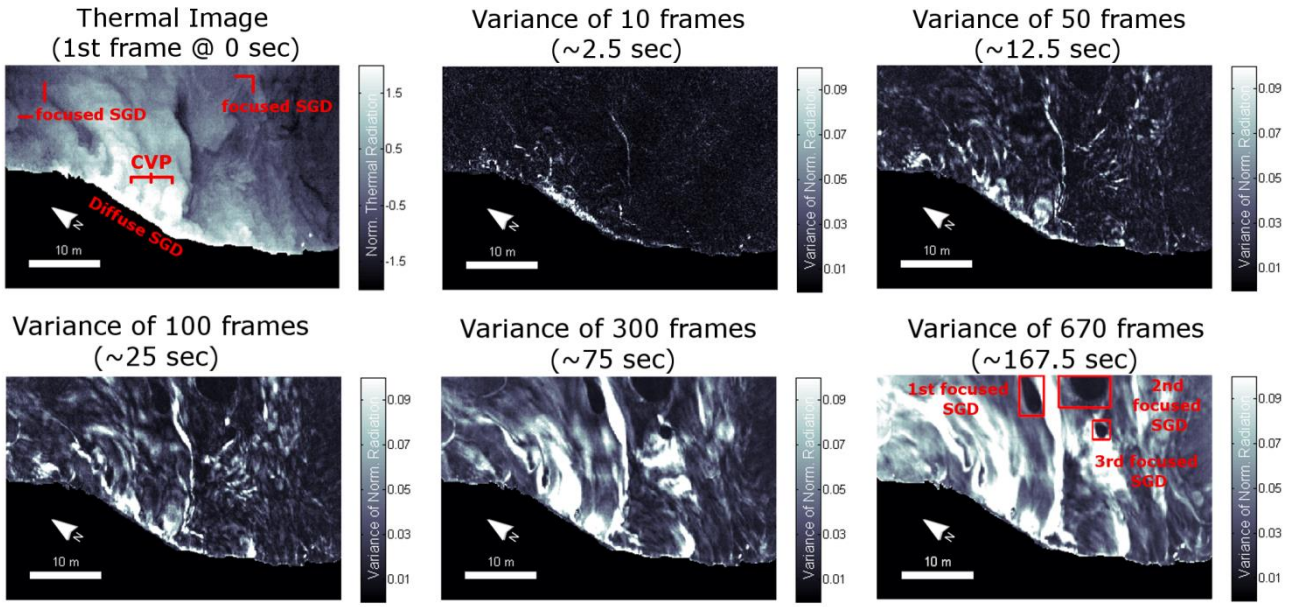

Figure 3: Variance of normalized thermal radiances over time starting with a normalized thermal radiance image (~~1st~~first frame) showing ~~indications~~ambiguous evidence of focused SGD spots, but distinct evidence of diffuse SGD and counter rotating vortex pairs (CVP~~)~~). The latter serves as an indication of a focused flow within the diffuse SGD area (upper left panel). The following panels show the integration of 10, 50, 100, 300, and 670 frames as variance per pixel. The final image (lower right panel) shows three delineated focused SGD spots (red boxes) indicated through variance values <0.019.

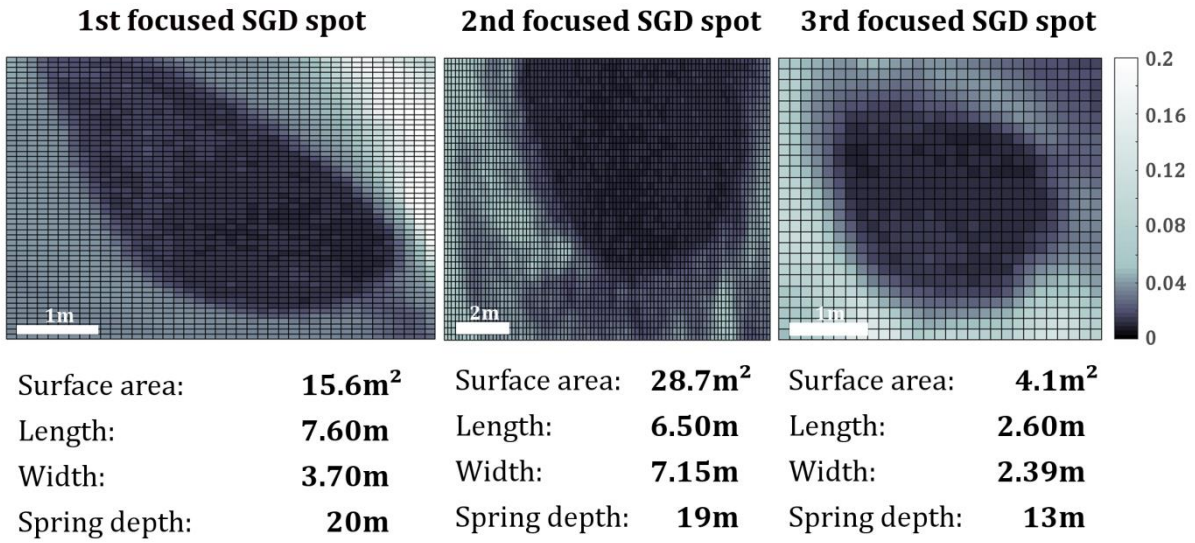

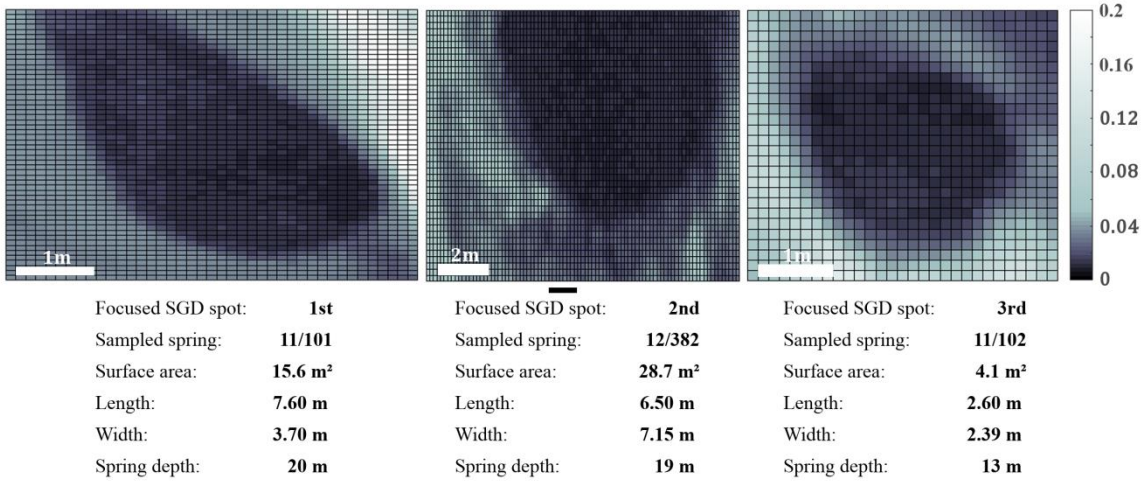

Figure 4: Spatial characteristics of the ~~three~~presented focused SGD spots ~~elaborated~~ and ~~focused on~~their spatial correspondence of sampled submarine springs during ~~the present study~~previous campaigns.

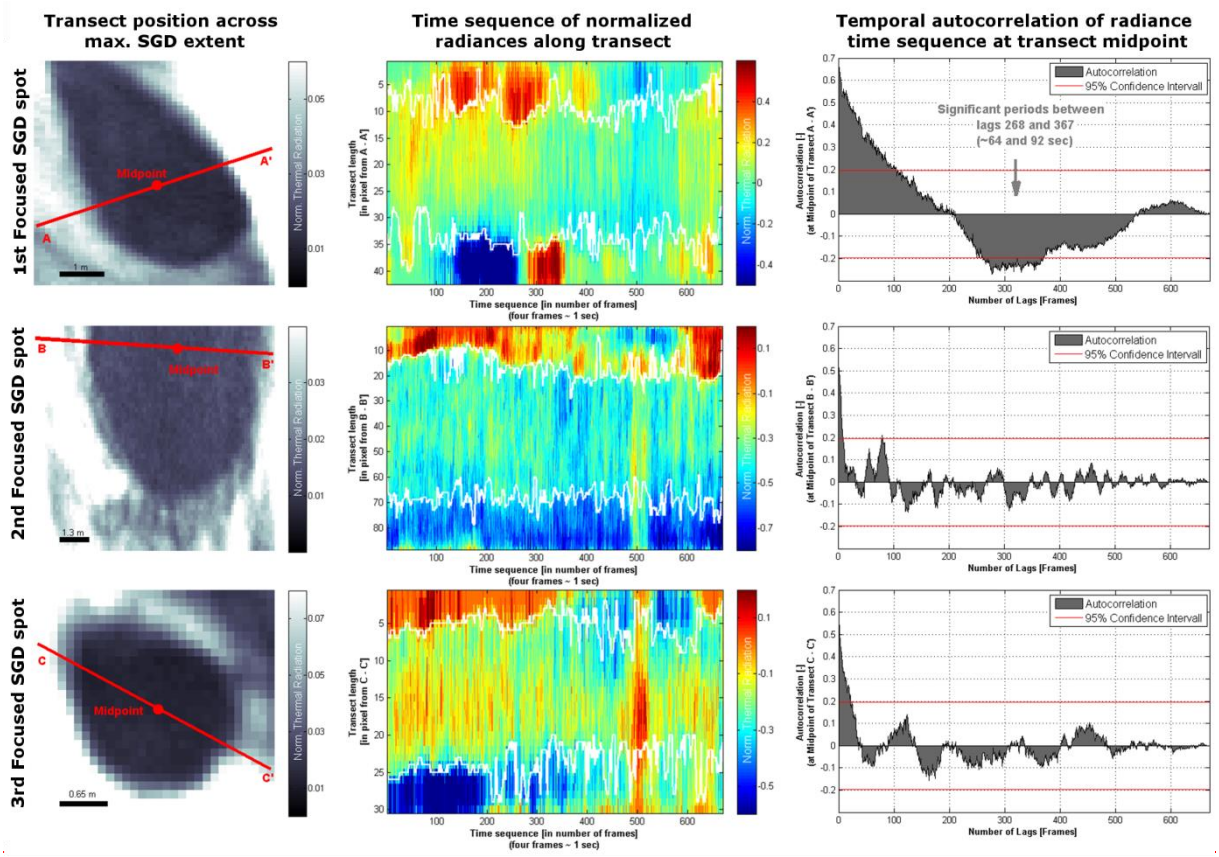
Transect position across max. SGD extent
Time sequence of normalized radiances along transect
Temporal autocorrelation of radiance time sequence at transect midpoint
1st Focused SGD spot
2nd Focused SGD spot
3rd Focused SGD spot
Midpoint
A
A'
B
B'
C
C'
1 m
1.3 m
0.65 m
Norm. Thermal Radiation
Transect length [in pixel from A - A']
Transect length [in pixel from B - B']
Transect length [in pixel from C - C']
Time sequence [in number of frames] (four frames ~ 1 sec)
Autocorrelation
95% Confidence Intervall
Significant periods between lags 268 and 367 (~64 and 92 sec)
Autocorrelation [-] (at Midpoint of Transect A - A')
Autocorrelation [-] (at Midpoint of Transect B - B')
Autocorrelation [-] (at Midpoint of Transect C - C')
Number of Lags [Frames]

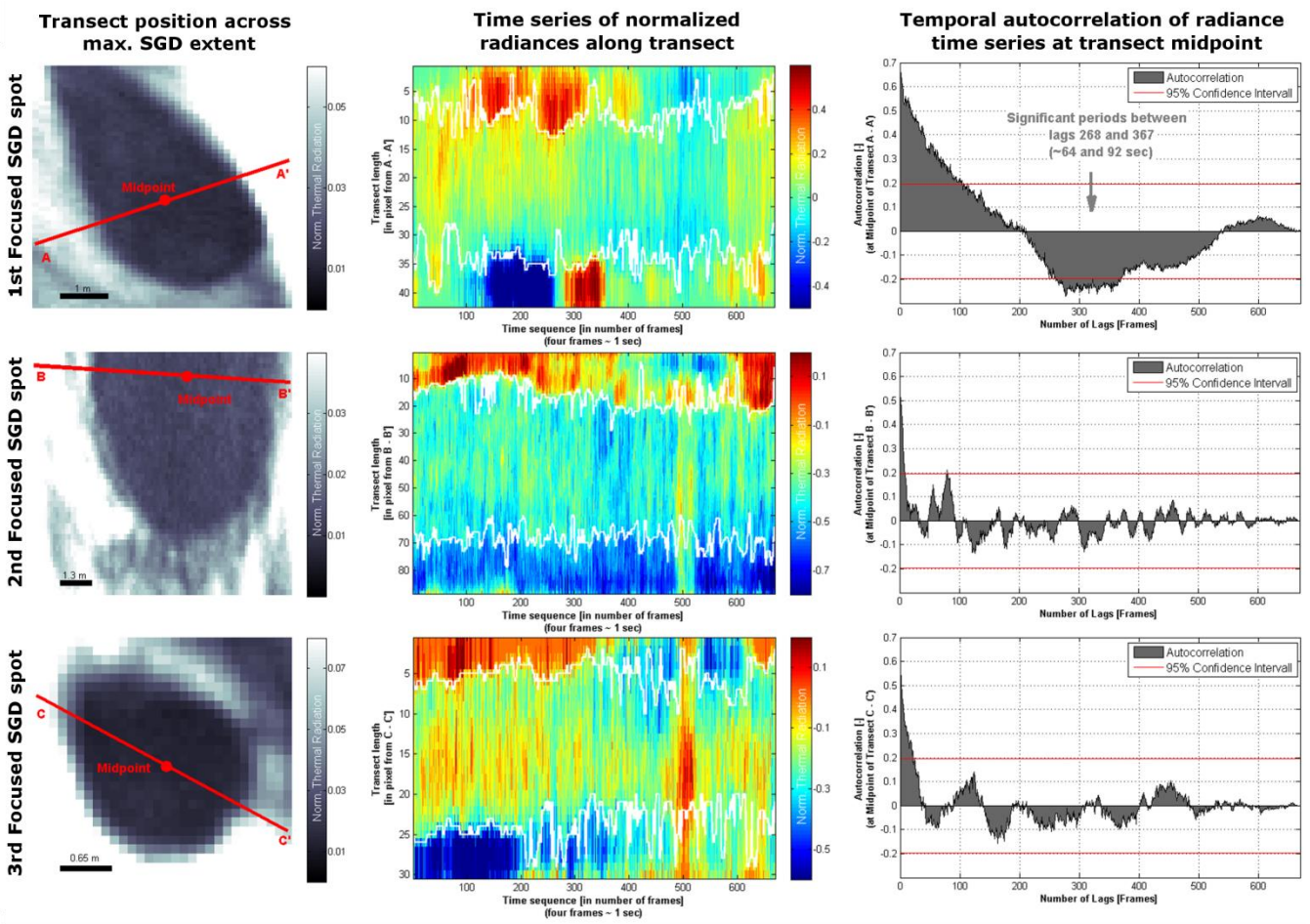

Figure 5: Analyses of spatiotemporal behavior and potential periodicity of SGD spots are presented. The first column shows transects across the maximum extent and midpoint position of SGD spot (subsets correspond to the red boxes shown in Fig. 43; note that the spatial scale varies between each spot indicated through the scale bar at the lower left of each subset). The middle column shows the normalized thermal radiance (NTR) values along transects over time. The white lines indicate the boundary of the focused SGD spots. The third column shows the temporal autocorrelation of the ~~normalized radiance~~NTR values along the entire ~~frame set (~~time ~~sequence)~~series obtained at the midpoint of transect as described in section 2 to detect possible periodicities.

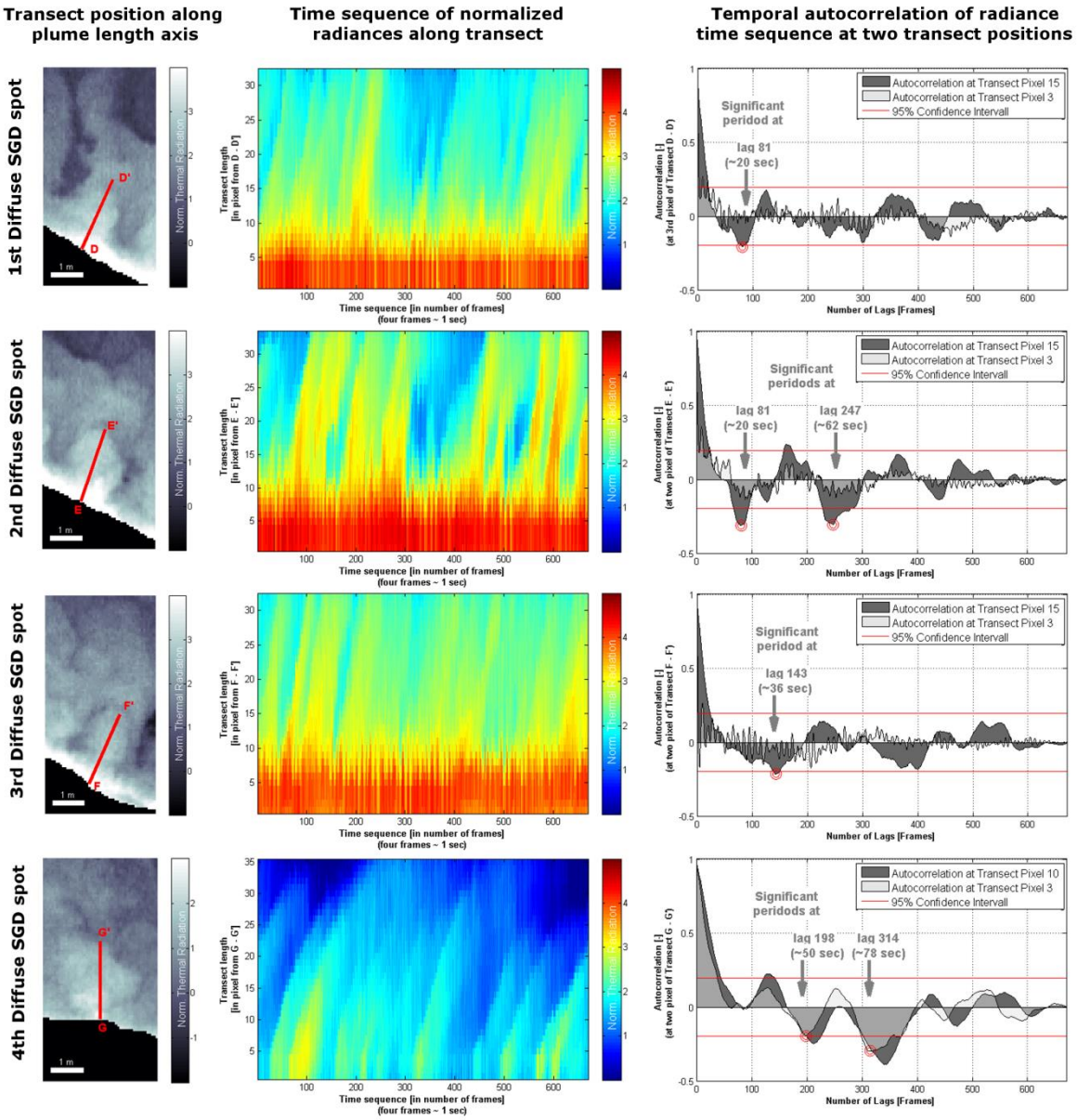
Transect position along plume length axis
Time sequence of normalized radiances along transect
Temporal autocorrelation of radiance time sequence at two transect positions
1st Diffuse SGD spot
2nd Diffuse SGD spot
3rd Diffuse SGD spot
4th Diffuse SGD spot
Norm. Thermal Radiation
Transect length [in pixel from D - D']
Transect length [in pixel from E - E']
Transect length [in pixel from F - F']
Transect length [in pixel from G - G']
Time sequence [in number of frames] (four frames ~ 1 sec)
Autocorrelation at Transect Pixel 15
Autocorrelation at Transect Pixel 3
Autocorrelation at Transect Pixel 10
95% Confidence Intervall
Significant peridod at
Significant peridods at
lag 81 (~20 sec)
lag 247 (~62 sec)
lag 143 (~36 sec)
lag 198 (~50 sec)
lag 314 (~78 sec)
Autocorrelation [-] (at 3rd pixel of Transect D - D')
Autocorrelation [-] (at two pixel of Transect E - E')
Autocorrelation [-] (at two pixel of Transect F - F')
Autocorrelation [-] (at two pixel of Transect G - G')
Number of Lags [Frames]

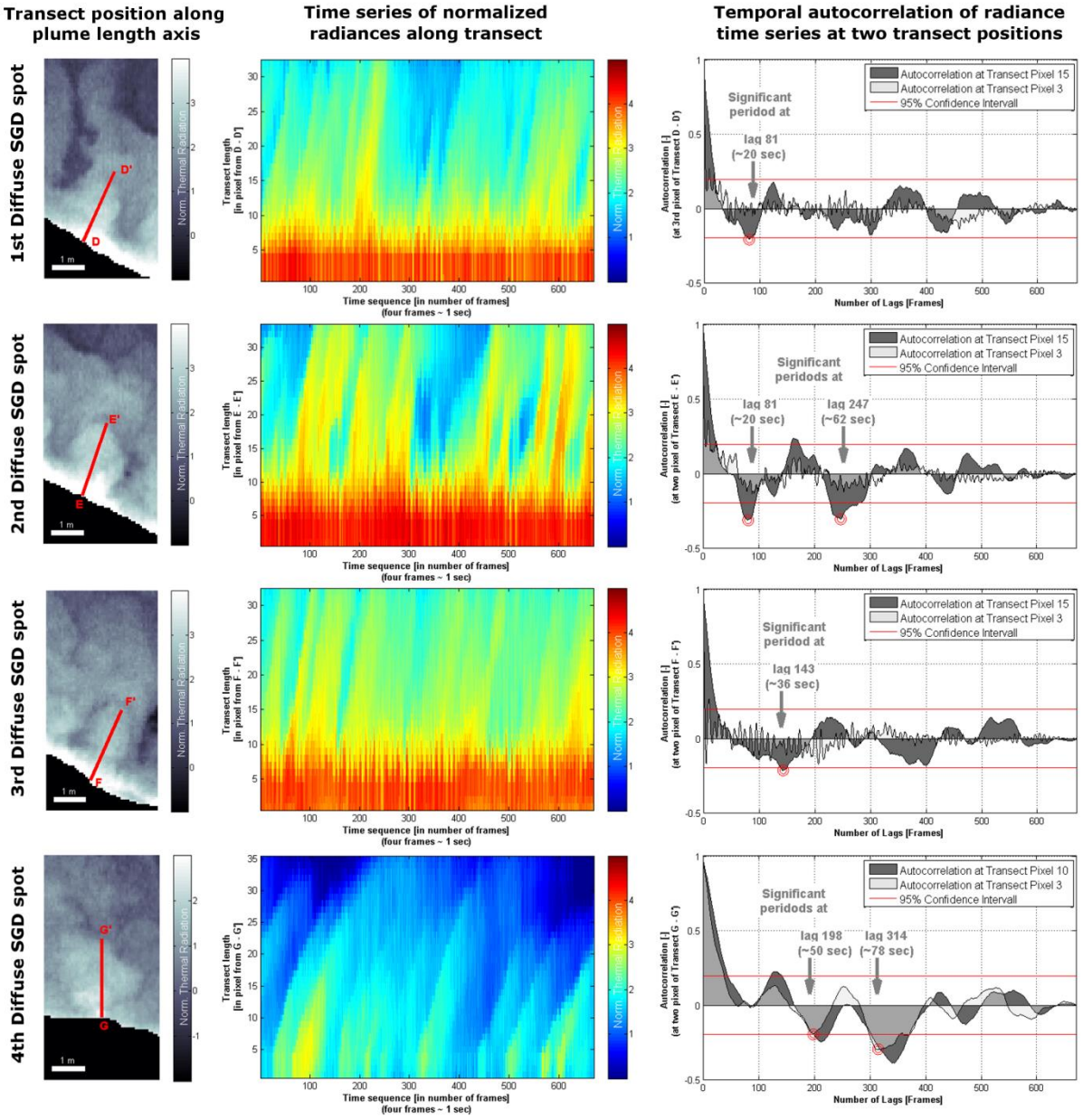

Figure 6: Analyses of spatiotemporal behavior and potential periodicity of diffuse SGD spots are presented. The first column shows transects across the maximum extent and midpoint position of diffuse SGD spots (note that the spatial scale varies between each spot indicated through the scale bar at the lower left of each subset). The middle column shows the normalized thermal radiance (NTR) values along transects over time. The third column shows the temporal autocorrelation of ~~the normalized radiance~~NTR values along the entire ~~frame set (~~time ~~sequence)~~series obtained at the midpoint of the transect. Those points reflect the ~~clearest and mostly pristine~~most unaltered discharge signals (the larger value). As reference, we show the third transect pixel (close to the shoreline) as well in order to outline the wave influence on the periodicity.

Table 1: Summary of values characterizing the spatiotemporal behaviour of each focused and diffuse SGD spot

	SGD spot	Boundary distance*Corresponds to sampled spring	Spatial variation* [in %]	Peak Values** (standard deviation)	Distinctive featureSignificant Periodicity	Significant Period [in sec]
		~~[in pixel]~~ ~~[in meter]~~	~~[in %]~~			
focused	1st	20-3111/101	55155.0	0.08 - 0.24 (0.11))***	Higher peak values during frames 100-300 and 500-670 and lower during frames 301-499Yes	64-92
	2nd	12/382	39139.5	-0.17- -0.26 (0.09))***	Exceptional peak values during frames 485-520Yes	20
	3rd	11/102	116.7	-0.08 - 0.06 (0.07)***	No	-

diffuse	1	-	150.0	2.99 – 4.52 (0.22)***	Yes	20
	2	-	266.0	3.54-4.71 (0.17)***	Yes	20, 62
	3	-	150.0	3.31-4.36 (0.17)***	Yes	36
	4	-	600.0	1.37-3.17 (0.39)***	Yes	50, 78

* For 90% of the data

** Mean of the maximum values per frame over time

*** P-value of <0.001 according to a Wilcoxon rank sum test, testing the significance of the peak values against non-peak values

Table 2: Water chemistry of all sampled focused SGD and onshore ~~springs~~springs, along with the result from the inverse geochemical ~~modeling~~modelling and the volumetric calculation~~.~~. Note that the volumetric calculation is based on the molar volume of halite (29.24 cm^3/mol), aragonite (34.17 cm^3/mol) and gypsum (74.29 cm^3/mol). Also note that the information given here represents a summary of the most important information. Full details are given in Tables S2 in the supplementary material.

	Analytical Results				Modelling Results				Volumetric Calculation			
	T [°C]	pH [-]	TDS [g/l]	Density [g/cm^3]	Interstitial Brine [kg]	Halite [mol/kgw]	Aragonite [mol/kgw]	Gypsum [mol/kgw]	Halite [cm^3/m^3 H_2O]	Aragonite [cm^3/m^3 H_2O]	Gypsum [cm^3/m^3 H_2O]	Sum
Interstitial Brine												
	35.6	5.38	345	1.23								
Onshore Springs												
09/854	27.9	7.20	7.3	1.00	0.012	0.0123	0.0017	0.0017	359.5	59.5	125.7	544.7
09/855	28.5	7.12	26.0	1.00	0.049	0	0.0017	0.0201	0	59.4	1493.0	1552.4
09/856	28.1	7.16	15.6	1.00	0.028	0	0.0019	0.0087	0	65.3	649.4	714.7
09/857	27.6	7.11	21.2	1.00	0.039	0	0.0017	0	0	59.0	0.0	59.0
09/858	27.6	7.48	6.4	1.00	0.011	0.0071	0.0020	0.0016	208.3	69.5	119.8	397.6
Focused SGD												
11/120	29.6	7.25	15.8	1.00	0.030	0	0.0025	0.0071	0	85.5	527.1	612.6
10/30	28.0	6.75	9.5	1.00	0.201	0	0	0.0011	0	0	79.8	79.8
12/382	31.5	7.27	8.7	1.00	0.015	0.0056	0.0021	0.0024	163.4	73.3	177.3	414.0
11/126	30.0	7.37	4.9	1.00	0.008	0.0051	0.0021	0.0012	150.0	71.6	88.0	309.6
11/101	24.0	7.16	12.8	1.00	0.022	0.0109	0.0036	0.0034	319.3	122.3	254.8	696.5
11/102	26.6	7.24	13.9	1.00	0.025	0.0125	0.0032	0.0037	365.6	110.3	273.8	749.7
11/121	21.0	7.08	24.8	1.00	0.048	0	0.0018	0	0	62.4	0	62.4